ABSTRACT

KARIMI-MOGHADDAM, GITI. Applications of Thermomagnetic Convection in Thermal Management of Electronic Systems. (Under the direction of Dr. Richard D. Gould and Dr. Subhashish Bhattacharya).

A ferrofluid is an electrically nonconductive colloidal suspension consisting of a carrier liquid and magnetic nanoparticles. The novelty of ferrofluids is that the fluid flow and properties may be controlled by an external magnetic field and thermal field. Since the discovery of the unique properties of ferrofluids, several applications for ferrofluids have been considered; the variety of applications is diverse, ranging from biomedical and technical to scientific applications.

In this thesis, the thermomagnetic convection effect of a ferrofluid in a differentially heated flow loop under the influence of an external magnetic field has been investigated analytically, numerically and experimentally. The physics of thermomagnetic convection is a highly multi-disciplinary area, which combines fluid dynamics and heat transfer with magnetism. This application utilizes ferrofluids whose magnetic properties are strongly influenced by temperature which are called temperature sensitive ferrofluids (TSFF) in this study. When a temperature sensitive ferrofluid experiences a temperature variation in the presence of an external magnetic field, the balance of the induced magnetic body force is broken and a thermomagnetic driving force is produced.

The objective of this research is to characterize the thermomagnetic circulation through a flow loop in terms of geometric length scales, ferrofluid properties, and the strength of the imposed magnetic field with the goal to provide a practical design approach for liquid cooling of electronics using of thermomagnetic effect of ferrofluids with no mechanical pump.

In the analytical study, a one-dimensional model has been developed using scaling arguments to characterize thermomagnetic circulation in a flow loop in terms of physical parameters. Accordingly, a correlation for the non-dimensional heat transfer (Nusselt number) as a function of the appropriate magnetic Rayleigh number and a correlation for the mass flow rate based on the system properties (magnetic Grashof number) were developed.

In parallel to the analytical analysis, thermomagnetic circulation flow loops were investigated numerically. The experimentally validated three-dimensional, incompressible, laminar numerical simulation models included the heat transfer process from a temperature sensitive ferrofluid contained in a closed flow loop under the influence of an external magnetic field. These models were established using COMSOL Multiphysics simulation software which in addition to solving the standard conservation equations, also solve for the magnetic field inside the simulation domain using the Maxwell equations, and include the necessary terms to take into account the magnetic body force to add to the momentum equation. Results of these numerical investigations have been used to develop semi-empirical analytical correlations. Additionally, the effect of relative positions of the heat source and the magnetic field source on system performance has been studied by considering six different cases.

The experimental measurements using a single-phase, temperature sensitive ferrofluid (TMA-250) operating under transient and steady-state laminar flow conditions in a partially heated thermomagnetic circulation flow loop under the influence of the magnetic field were used to validate the analytical and numerical studies. The cooling performance of the device with different magnetic field strengths and heating rates on the heating section were investigated. The results have revealed that flow in these devices can be controlled by the magnetic field and temperature distribution, and that the device possesses a self-regulating

function corresponding to the heat source heat rate. This feature may be used as a self-regulating cooling device for thermal management of electronics without the need for a mechanical pump or sensors and an external control system.

Applications of Thermomagnetic Convection in Thermal Management of Electronic Systems

by
Giti Karimi-Moghaddam

A dissertation submitted to the Graduate Faculty of
North Carolina State University
in partial fulfillment of the
requirements for the degree of
Doctor of Philosophy

Mechanical Engineering

Raleigh, North Carolina

2014

APPROVED BY:

_____	_____
Dr. Richard Gould	Dr. Subhashish Bhattacharya
Co-Chair of Advisory Committee	Co-Chair of Advisory Committee
_____	_____
Dr. Alexei Saveliev	Dr. Tarek Echekki
_____	
Dr. Douglas Hopkins	

DEDICATION

This dissertation is dedicated to all those

whom I love, especially

My dear husband, Amir,

My mother, Fakhri,

and

the memory of my father, Hasan

BIOGRAPHY

Giti Karimi-Moghaddam is a Ph.D. student in the Department of Mechanical and Aerospace Engineering at North Carolina State University. She received the Bachelor of Science degree in Mechanical Engineering from Shahrood University of Technology in 2006 and the Master of Science degree in Energy Systems Engineering from Sharif University of Technology in 2009. During her years at NC State University, she served as a research assistant in the FREEDM center and Department of Electrical and Computer Engineering and as a teaching and research assistant in Department of Mechanical and Aerospace Engineering. Her research interests include analytical and theoretical analysis, numerical modeling, simulation and experimental examination of advanced thermal management techniques for electronic systems and electromagnetic devices.

ACKNOWLEDGMENTS

I would like to express my deepest gratitude to my advisors, Dr. Richard Gould and Dr. Subhashish Bhattacharya, for their utmost support and thoughtful guidance during the course of preparing this dissertation. My special thanks go to Dr. Echekki, Dr. Saveliev, and Dr. Hopkins for serving on my committee and for all the constructive comments they have given me on this work. I would like to express my sincere gratitude to my husband for his continuous support and encouragement during my studies.

TABLE OF CONTENTS

LIST OF TABLES

LIST OF FIGURES

1 Introduction

To remain competitive, power electronic manufacturers are increasing power density in electronic systems. However, the power density which can be achieved in electrical devices is mainly thermally limited. Therefore improving the cooling efficiency generally will lead to an improved performance. Different thermal management solutions for electronic systems have been proposed and implemented along the years. However, these cooling approaches usually add a reliability, weight, space, cost, power density and/or maintenance penalty.

Liquid cooling for thermal management has been widely applied in electronic systems; several efficient liquid cooling techniques like micro jet cooling devices and spray coolers are very efficient. However they require the use of a mechanical pump which may often introduce reliability and mechanical limitations such as vibration, noise and leakage problems, considerable power consumption, and maintenance because of moving parts.

During the last decades, liquid transport systems without mechanical pumps have been proposed in which the fluid flow can be achieved by virtue of some new concepts for driving them and there has been some noticeable progresses. A typical actuator developed using an electrostatic force [1] which results in a reciprocating motion of a membrane to drive the fluid where the flow direction is controlled by two passive check valves. Later some other driving principles were used with this membrane structure to form different actuators for example magnetic actuators [2], piezoelectric actuators [3], thermo-pneumatic actuators [4], and shape memory alloy actuators [5]. Although these methods allowed for a thinner design and drive liquid in one direction, there still is the risk of fatigue in the passive check valves

and of valve clogging. Therefore valve-less actuators were investigated in which diffuser elements were used for direction control [6]. However, there were still moving parts (i.e. membranes) in these reciprocating based actuators and the reliability problem was a concerned. Additionally the pulsating flow rates may produce temperature fluctuations and so reduce the stability of the electronic device. A popular type of fluid control system with no moving parts is the well-known capillary pumped loop (CPL) [7]. This approach relies on the surface tension forces induced by a fine pore wick to drive the working fluid. Such a two-phase system uses the same basic principle as heat pipes (i.e. closed evaporation-condensation cycle being maintained by capillary pumping [8]). Although there are no moving parts in a CPL, they can become unstable due to pressure oscillation, startup failure, gravity dependence and an unexpected change of the power in the evaporator which can cause severe performance degradation of the whole system [8].

With regard to liquid cooling applications having no mechanical pump, field induced flow systems have been attractive. In these systems pumping forces result due to the interaction between electromagnetic fields and the fluid. The study of various field and fluid interactions may be divided into three main categories [9];

- electrohydrodynamics (EHD), which deals with electric force effects
- magnetohydrodynamics (MHD), which deals with the interaction between magnetic fields and fluid conductors of electricity, and
- ferrohydrodynamics (FHD), which deals with the mechanics of fluid motion induced by forces of magnetic polarization

EHD applies the Coulomb force (the force due to free electric charge acted upon by an electric force field [9]) on a low electrical conductivity fluid [10, 11] . Actuators based on EHD have no moving parts and their structures are simple, but the choice of a suitable working fluid is limited by their electrical conductivity [10, 11]. In MHD, the body force acting on the fluid is the Lorentz force which arises when an electric current flows at an angle to the direction of an applied magnetic field [9]. Contrary to the EHD actuators, the working fluids in MHD systems are limited to fluids with very high electric conductivity [10, 11]. Focusing on liquid metals applications with MHD systems, reasonable forces for providing significant liquid metal flow (with high viscosity) require extremely high magnetic field strength on the order of several Tesla [3]. A liquid metal require usually a high temperature environment, therefore it does not fit the requirements for a broad technical application [12, 13].

In FHD there is no need for electric current flow in the fluid thus working fluid is usually electrically nonconductive. The body force in FHD is due to material magnetization in the presence of magnetic field gradients which is known as the Kelvin body force [12, 13]. FHD is the basis of a simpler fluid control system design which will be explained more comprehensively below.

In the early to mid-1960s Ferrohydrodynamics began to be developed, initially motivated by the objective of converting heat to work using no mechanical parts [9]. However, as colloidal magnetic fluids (ferrofluids (FF)) became available many other applications of these fascinating liquids were recognized under FHD effects. One of these applications is known as

thermomagnetic convection [9], which exploits the temperature sensitivity of the FF under an external magnetic field gradient.

A FF is an electrically nonconductive, colloidal suspension consisting of ferro or ferrimagnetic single domain nano-scale particles (such as iron, cobalt, nickel, manganese, copper or zinc) in a liquid carrier (such as oil, transformer oil, kerosene, diester, hydrocarbon, fluorocarbon, water) [9]. In the absence of an applied magnetic field, the particles inside the FF are randomly oriented and the fluid has no net magnetization. The FF can be magnetized by an external magnetic field, aligning the magnetic moment of the particles with the applied magnetic field direction. The strength of the resulting magnetization depends on the applied magnetic field strength and on the fluid temperature. One of the particularities of FFs is that their magnetization decreases with increasing temperature [12, 13]. Therefore, once a FF experiences a temperature variation in the presence of an external magnetic field, the fluid behaves as a "smart fluid" [9] and will experience a larger magnetization in the low temperature region than that in the high temperature region, consequently a net magnetic driving force can be produced to drive the fluid to flow toward the heated region, which is the principle of thermomagnetic convection [9]. The main application of this phenomena, which is investigated in this thesis, is related to the use of FFs as a heat transfer medium. FFs have been used to enhance the heat transfer, especially in electromagnetic and electronic devices, where the presence of a magnetic field and magnetic field gradient causes thermomagnetic convection [11, 14-16]. Cooling based on thermomagnetic convection is particularly useful in systems used in low gravity space

applications, where gravitational convection is absent, or in systems in which the natural circulation should occur against gravity or independent of the position of the device.

Numerous numerical and experimental studies considering thermomagnetic effects of temperature sensitive magnetic fluids have been conducted [11, 14, 15, 17-23]. Theoretical and experimental studies were carried out to investigate self-flowing energy transport devices based on the thermomagnetic circulation of a temperature sensitive magnetic fluid in a loop type flow [11, 15, 19, 20, 24], and also in a square enclosure with localized heat sources [14, 18, 21]. Despite the many studies, there still is a lack of understanding of when a FF can be used for effective cooling; primarily because many of these studies use dimensional parameters, which makes scaling and design difficult. Although there are some studies where scaling analysis is used to characterize thermomagnetic convection in enclosures filled with a FF [14, 18, 21], to our best knowledge, there are no previous efforts to examine thermomagnetic circulation flow loops using dimensionless parameters.

The objective of this research is to characterize the thermomagnetic convection in a differentially heated flow loop under the influence of an external magnetic field using dimensional analysis in terms of geometric length scales, magnetic fluid properties, and the strength of the imposed magnetic field and to provide a practical design approach for liquid cooling using the thermomagnetic effect of FFs. In order to do this, studies have been carried out in three groups including, i.) an analytical study, ii.) numerical simulations, and iii.) experimental measurements.

In the analytical study, a one-dimensional theoretical model has been developed using scaling arguments to characterize a thermomagnetic circulation loop in terms of physical

parameters. Accordingly, a correlation for the non-dimensional heat transfer (Nusselt number) as a function of the appropriate magnetic Rayleigh number and a correlation for the mass flow rate based on the system properties were developed. Additionally, some of the practical application limitations were discussed in this part.

In parallel to the analytical study, thermomagnetic circulation flow loops were investigated numerically. The three-dimensional, incompressible and laminar conservation equations used here include equations of motion as well as the energy equation for a temperature sensitive ferrofluid contained in a closed flow loop under the influence of an external magnetic field where solved. COMSOL Multiphysics simulation software version 4.4 was used to solve a set of coupled partial differential equations (PDEs) using the finite element method [25], which in addition to solving the standard conservation equations, also solve for the magnetic field inside the simulation domain using the Maxwell equations, and include the necessary terms to take into account the magnetic body force have been added to the momentum equation. Numerical simulations were conducted to investigate the effects of different flow loop diameters, magnetic fields strengths, and heating loads. These simulations have been validated against experimental results. Moreover, the effect of the relative positions of the heat source and the magnetic field source on the performance of the thermomagnetic circulation flow loop have also been studied numerically.

Experimental measurments using a single-phase, temperature sensitive magnetic fluid (Mn-Zn ferrite based) operating under steady-state laminar flow conditions in a partially heated thermomagnetic circulation flow loop under the influence of an external magnetic field where used to validate the theoretical and numerical studies. Additionally, this experimental

work documents a range of operational conditions for a practical thermomagnetic circulation loop used for electronic cooling. The cooling performance of the device with different magnetic field strengths and heating rates were investigated to determine the feasibility of using such devices for the thermal management of electronic systems.

Accordingly, the thesis has been organized as follows:

In Chapter 2 a detailed description of magnetic fluids, including structural parameters, fabriaction approaches, characteristics of ferrofluids and their variation with fluid parameters and strength of the external magnetic field are presented. In addition, this chapter describes the concept of the thermomagnetic driven flows, and also includes a review of similar work in this field.

Chapter 3 is devoted to the 1-D analytical model and presents the analytical approach, basic assumptions, the geometry and the boundary conditions of the problem. This chapter concludes by introducing the dimensional parameters and scaling arguments used to characterize the thermomagnetic circulation flow loop. Finally, some of practical limitations of such a cooling system are discussed.

Chapter 4 includes the numerical simulation of the thermomagnetic circulation flow loop. This chapter gives a description of the numerical method, geometry and boundary conditions used in this study. Numerical results are validated using the experimental measurments results. the effect of the relative positions of the heat source and the magnetic field source on the performance of the flow system has also been investigated.

In Chapter 5, the experimental setup of the thermomagnetic cooling device is described. This chapter presents the details of the prototype and its components. In addition, the operational

conditions and test results using the experimental apparatus are reported in this part of the thesis.

Finally, Chapter 6 concludes the works including some suggestions for future investigations in this field.

2 Research background

2.1 Magnetic fluids

Magnetic fluids may be classified as ferrofluids (FF), which are colloidal suspensions of very fine (nano scale) magnetic particles, and magnetorheological fluids (MR), which are suspensions of larger (micron scale), usually non-stable, magnetic particles [26, 27]. MR fluids differ in one major respect from FFs in that they undergo large changes in their rheological properties (i.e. liquid to solid transition), when exposed to a magnetic field, while FFs remain flowable in the presence of magnetic field even when magnetized to saturation [9]. This research deals with the study of FFs and their application in liquid cooling of electronic systems. Before we discuss the application of FFs as thermomagnetic convection in this thesis, we will first have a glance on their basic make-up, stability requirements, magnetization mechanisms, and physical properties.

A ferrofluid is an electrically nonconductive, colloidal suspension consisting of ferro or ferrimagnetic single domain nano-scale particles (Ferrites are a class of ferromagnetic materials represented by the general formula $M^{2+}OFe^{3+}O_3$, where M is a metal such as iron, cobalt, nickel, manganese, copper, zinc or a combination of them) in a liquid carrier. The liquid carrier could be an oil, transformer oil, kerosene, diester, hydrocarbon, fluorocarbon or even water [9, 16]. A range of properties can be obtained through the choice of ferrite particles (M in the mentioned formula), which may be a single metal species or a combination of two or more species [26]. The resultant behavior of this fluid, termed super-

paramagnetism, is similar to paramagnetism except that the magnetization in low to moderate fields is much larger [9].

There are essentially two methods to prepare the nanoparticles for ferrofluids; (i) by size reduction [28], which magnetic powder of micron size is mixed with a solvent and a dispersant in a ball mill in order to grind for a period of several weeks. (ii) chemical precipitation [9], which is probably the most used method to prepare magnetic nanoparticles. In general, this procedure starts with a mixture of $FeCl_2$ and $FeCl_3$ and water. Co-precipitation occurs with the addition of ammonium hydroxide, and then the system is subjected to different procedures to peptization, magnetic separation, filtration and finally dilution [9].

In order to avoid agglomeration of particles, the magnetic particles have to be coated with a shell of an appropriate material. According to the coating, the FFs are classified into two main groups: (i) surfacted ferrofluid (SFF) that the coating is a surfactant molecule, and (ii) ionic ferrpfluid (IFF) which is an electric shell [27].

Surfacted ferrofluids (which are mostly related to our application) are formed by magnetic particles coated with surfactant agents (amphiphilic molecules, as oleic acid) in order to prevent their aggregation. Steric repulsion between particles acts as a physical barrier that keeps grains in the solution and stabilizes the colloid [9]. In ionic ferrofluids, nanoparticles are electrically charged to keep the colloidal system stable. Figure 2-1 shows a schematic of surfacted magnetic nanoparticles.

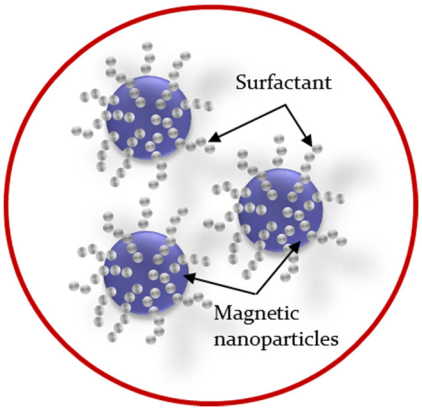

Figure 2-1 Surfacted magnetic nanoparticles

2.2 Stability requirements

Stability as a colloidal is an important property that ensures the suitability of a FF for fluid applications as well as for scientific studies. A magnetic particle in suspension is subject to various influences, some of which work to keep the particle in free suspension, and others of which tend to undermine the stability of the FF by causing the particles to clump or settle out. The first criteria of stability include the stability against sedimentation of the particles. Such sedimentation and the associated remixing of the suspensions can be determined by gravitational or magnetic forces. Therefore, to prevent the particles sedimentation and to remain the suspension well dispersed, the thermal energy of the particles needs to be high enough to provide sufficient mixing of the suspensions. Thus it requires being higher than the energy of the particles in the gravitational field or in a magnetic field, respectively [9].

For investigation the criteria of physicochemical stability, a dimensional approach has been used. Expressions for various energy terms per particle are used in this method as [9]:

$E_T = k_B T$ Thermal energy (2.1)

$E_M = \mu_0 M_d HV$ Magnetic energy (2.2)

$E_G = \Delta\rho V g L$ Gravitational energy (2.3)

where $k_B, T, \mu_0, M, H, V, \Delta\rho, g,$ and L are Boltzmann constant (1.38×10^{-23} J/K), absolute temperature (K), the permeability of free space ($4\pi\times10^{-7}$ N/A^2), magnetization of magnetic material (A/m), magnetic field intensity (A/m), particle's volume ($\pi d^3/6$ m^3) for a spherical particle of diameter d, density difference between the particles and the carrier liquid (kg/m^3), gravitational acceleration (9.81 m/s^2), and the elevation in the gravitational field, respectively [9, 27]. Ratios of one term to another give dimensionless quantities that can alter the stability of the FFs. This approach is explained in the following.

2.2.1 Stability in a magnetic field gradient

Considering the stability against settling of particles in an external magnetic field gradient, particles are attracted to the region with higher intensity of magnetic field, while thermal motion counteracts the field force and provides statistical motions that allow the particles to diffuse all portions of the fluid volume [9]. In other word, the sedimentation in magnetic field can be avoided as long as the thermal energy is strong enough to enable the particles to move freely between a region with strong magnetic field and a field free region, thus stability against segregation is favored by a high ratio of the thermal energy to the magnetic energy [9]:

$$\frac{Thermal\ energy}{Magnetic\ energy} = \frac{k_B T}{\mu_0 M_d HV} \geq 1. \quad (2.4)$$

Rearranging and substituting for the volume of a spherical particle yields an expression for the maximum particle size [9]:

$$d \leq \left(\frac{6k_B T}{\pi \mu_0 M_d H}\right)^{1/3}. \tag{2.5}$$

Using a typical sample of FF with bulk material magnetization, M_d as 2×10^5 (A/m) which is placed in a magnetic field intensity, H as 5×10^4 (A/m) and temperature, T as 298 (K), the particle size computed from Eq. (2.5), is $d \leq 8.5\ nm$ [9].

2.2.2 Stability in gravitational field

Gravity continuously pulls an individual particle downward while thermal agitation tends to keep the particle dispersed throughout the fluid matrix. Although stability against gravity should be considered in regard to application of the FF, but normally gravity is less of a threat (in comparison with magnetic field effect) to the segregation of FFs in magnetically fluid control applications [9]:

$$\frac{Gravitational\ energy}{Thermal\ energy} = \frac{\Delta \rho g L}{\mu_0 M H} \ll 1. \tag{2.6}$$

2.2.3 Stability against magnetic particles agglomeration

According to previous sections, sedimentation stability of the suspension can be guaranteed by keeping a maximum diameter of the particles. Additionally agglomeration of the particles has to be avoided, because this would increase their active diameter and thus would cause a destabilization of the suspension by sedimentation [9].

The stability of the magnetic colloids against magnetic particles agglomeration depends on the thermal contribution and on the balance between attractive (Vander Waals and dipole-dipole) and repulsive (steric and electrostatic) interactions [9]. Besides thermal agitation to disrupt the agglomerates, the third essential ingredient of the colloidal FF (in addition to the

particles and the carrier liquid, as it was mentioned before) long chain molecular species on the particle surface (surfactant or ionic coating) prevents agglomeration of the particles by providing a steric repulsion between particles [9].

Considering all mechanisms which are correlated in the stability of a ferrofluid as a colloidal suspension magnetic fluid, the actual average size of the particles ranges up to about 10 nm [9].

2.3 Magnetism, relaxation mechanisms, and Curie temperature

2.3.1 Magnetism of ferrofluid

Magnetization theory for FF samples is based on the assumptions that FF consists of a collection of individual single domain (each particle with its embedded magnetic moment) ferromagnetic particles. The particles in the FF are analogous to the non-interacting molecules of a paramagnetic gas [9]. In the absence of an applied field, the particles are randomly oriented, and the fluid has no net magnetization. When the FF is stressed by a magnetic field the magnetic dipoles within the particles will attempt to align their magnetic dipole moment parallel to the direction of the applied field. This happens because the magnetic moments rotate to the minimum energy direction which is parallel to the field [9]. As the field magnitude is increased, the particles become more and more aligned with the field direction up to the magnetization achieves its saturation value (all particles are aligned with the magnetic field) [9]. Langevin's classical theory is applied to give the superparamagnetic relationships [9]; it is beginning with the torque $\vec{\Gamma}$ on a magnetic particle with magnetic moment $\vec{m}$ which is in an angle θ with an applied field $\vec{H}$ [9,29]:

$$\vec{\Gamma} = \mu_0 \vec{m} \times \vec{H} = \mu_0 m\, H \sin\theta. \quad (2.7)$$

Therefore, the energy of the particle is equal to the mechanical work required to rotate it through the angle θ [9]:

$$W = \int_0^\theta \Gamma d\theta = -\mu_0 mH\, [\cos\theta - 1]. \quad (2.8)$$

In Eq. (2.8), m is the magnitude of the particle's dipole moment, and defines as the ratio of the domain magnetization of the bulk magnetic material (which the particles are made of it) to the volume of the particle, assuming a spherical particle with diameter d [9]:

$$m = M_d V, \quad V = \frac{1}{6}\pi d^3. \quad (2.9)$$

While the dipole moment tends to align itself with the field, there is an additional thermal energy which counteracts this behavior and provides a randomizing spatial orientation. Using statistical thermodynamics this situation can be described by Boltzmann statistics which become the form [29]:

$$n = e^{-W/k_B T}, \quad (2.10)$$

where n is the number density of dipoles.

Substitution of Eq. (2.8) in Eq. (2.10) leads to the number density of dipoles (n):

$$n = e^{-\mu_0 mH/k_B T} e^{\mu_0 mH\cos\theta/k_B T} = n_0 e^{\mu_0 mH\cos\theta/k_B T}, \quad (2.11)$$

where n_0 denotes the amplitude of the number density of magnetic dipoles when the magnetic field is zero [9]. Integrating over an area as a sphere of radius R enclosing many magnetic dipoles (Figure 2-2) and dividing by the volume of the sphere gives the average number density of dipoles as below [9]:

$$N = \frac{1}{\frac{4}{3}\pi R^3}\int_{\theta=0}^{\pi}\int_{\varphi=0}^{2\pi}\int_{r=0}^{R} n_0\, e^{\mu_0 mH\cos\theta/k_BT} r^2 \sin\theta\, dr d\varphi d\theta = \frac{n_0}{\alpha}\sinh\alpha, \tag{2.12}$$

and:

$$\alpha = \frac{\mu_0 mH}{k_BT}, \tag{2.13}$$

where φ is the angle from the x-axis in the x-y plane [30], and α is the ratio of magnetic energy to thermal energy.

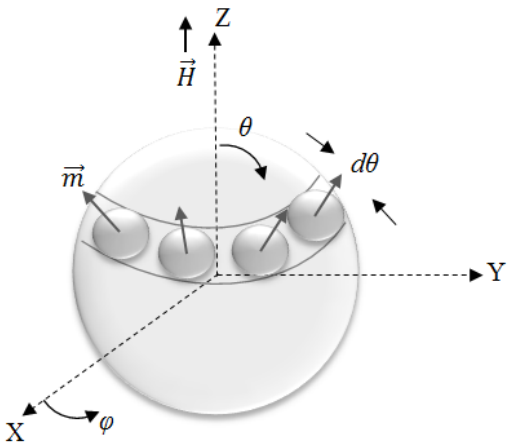

Figure 2-2 Contribution of magnetic dipoles with net magnetization [29]

As it is shown in Figure 2-2, the net magnetization will be parallel to direction of the applied magnetic field (here z direction), thus the magnetization in the x and y directions will average to zero over the sphere. The differential expression for the z directed magnetization M_z will be calculated as:

$$dM_z = \frac{mn}{\frac{4}{3}\pi R^3}\cos\theta\, r^2 \sin\theta\, dr d\theta d\varphi. \tag{2.14}$$

Substituting n from Eq. (2.11) in Eq. (2.14) and integrating over the volume of the sphere yields the Langevin equation for the superparamagnetic magnetization behavior of a colloidal ferrofluid (9, 27, 29):

$$\frac{M}{\phi M_d} = \frac{M}{M_s} = L(\alpha) = \coth(\alpha) - \frac{1}{\alpha} \ , \quad \left(\alpha = \frac{\mu_0 mH}{k_B T}\right) \tag{2.15}$$

where magnetization M of the ferrofluid has the direction of the applied field (Figure 2-2). Also ϕ, M_d, and M_s are the volume fraction of magnetic particles to liquid carrier, the domain magnetization of the bulk magnetic particle, and the saturation magnetization of the FF, respectively. Langavin equation implies the FF's magnetization as a function of the external magnetic field and temperature:

$$M = \frac{\vec{H}}{H} M(H,T) \tag{2.16}$$

The Langevin equation is plotted in Figure 2-3.

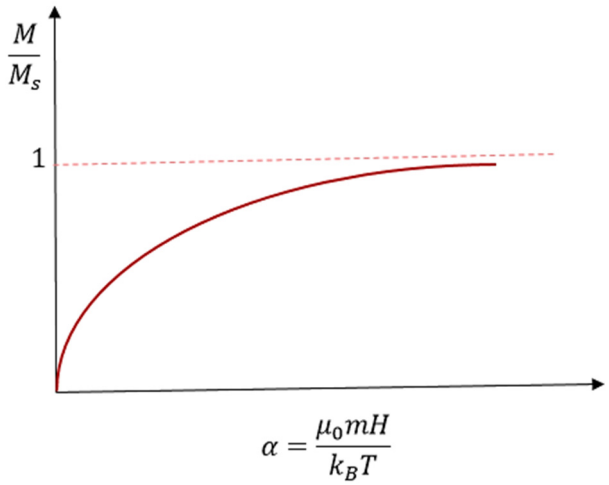

Figure 2-3 A typical theoretical Langevin equation

The asymptotic values of the Langevin function for small and large values of the parameter α using Taylor series expansions of Eq. (2.15) can be written as [9]:

$$\lim_{\alpha \to 0} L(\alpha) = \frac{M}{M_s} \approx \frac{\alpha}{3} = \frac{\pi}{18} \frac{\mu_0 M_d H d^3}{k_B T} \tag{2.17}$$

In the recent equations the magnitude of the dipole moment m, has been rewritten in terms of the domain magnetization and the particle volume using Eq. (2.9).

Eq. (2.17) as the low field limit, defines a linear relationship between the magnetization *M*, and the magnetic field *H*. The initial slope of the magnetization curve (Figure 2-3), x is defined as the magnetic susceptibility [9]:

$$x = \frac{M}{H} = \frac{\pi}{18} \frac{\mu_0 M_d M_s d^3}{k_B T} = \frac{\pi}{18} \frac{\mu_0 \phi {M_d}^2 d^3}{k_B T} \tag{2.18}$$

The initial susceptibility describes the magnitude of magnetic response shown by a FF at low field strengths [9]. A large value of *x* corresponds to strongly FF's magnetic response, while a small value corresponds to a weakly magnetic response of the FF to the external magnetic field (*x=0* for free space). Examination of Eq. (2.18) presents the same approximation is accurate at high temperatures [9]. In addition, the volume fraction of magnetic particles (ϕ) and also the size of particles (*d*) can play significant role in the initial magnetic response of the FF to the external magnetic field considering all other parameters are constant [9]. The magnetic susceptibility is related to the more common used magnetic permeability as:

$$\mu = (1 + x)\mu_0 \tag{2.19}$$

The high field limit of the Langevin equation (Eq. (2.15)), can be written as:

$$\lim_{\alpha\to\infty} L(\alpha) = \frac{M}{M_s} \approx 1 - \frac{1}{\alpha} = \left(1 - \frac{6}{\pi}\frac{k_B T}{\mu_0 M_d H d^3}\right). \quad (2.20)$$

Alternatively, a low temperature can also be used to work within this region. The high magnetic field region is also known as the saturation region because it describes the approach to a saturation value of magnetization at which all of the dipoles have aligned with the magnetic field [9].

2.3.2 Relaxation mechanisms

There are two distinct mechanisms for the rotation (relaxation) of the magnetic moments in the FF. One is Brownian rotation, which is the physical rotation of the particle into alignment with the magnetic field [9]. The other mechanism is Neel rotation, which is characterized by the movement of the particle magnetic moment with respect to the particle crystal axis (i.e. the rotation of the magnetic moment vector occurs within the particle (9)) [9]. These two processes are shown in Figure 2-4.

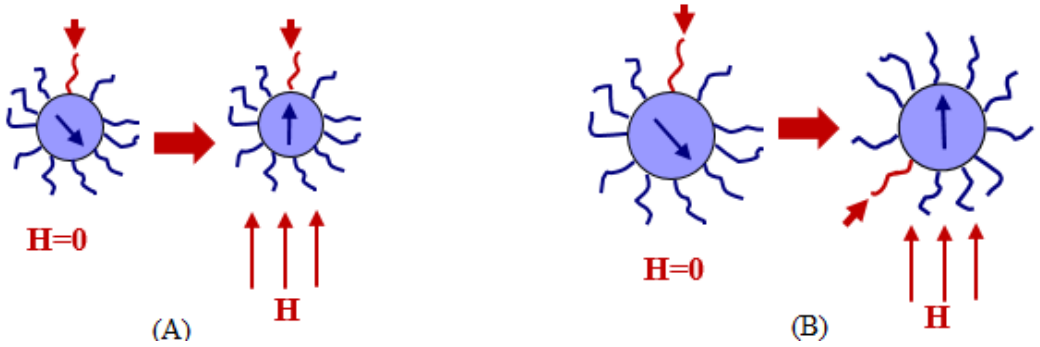

Figure 2-4 Magnetic relaxation mechanisms, (A) Neel relaxation, (B) Brownian relaxation

The particle size range within the FF and temperature are important since magnetic relaxation mechanisms are strongly dependent on these parameters [9]. The characteristic relaxation times for each mechanisms are given by [9]:

$$\tau_B = \frac{3V_B\eta}{k_BT}, \qquad \text{Brownian relaxation time} \qquad (2.21)$$

$$\tau_N = \frac{1}{f_0}e^{\frac{KV_N}{k_BT}}, \qquad \text{Neel relaxation time} \qquad (2.22)$$

where V_B, η, f_0, K, and V_N are Brownian particle volume (m^3) (considering the magnetic particle diameter and surfactant length), the carrier fluid dynamic viscosity (Pa.s), the frequency constant of Neel relaxation (Hz), the anisotropy constant of the particle, and Neel particle volume (m^3) (considering just the magnetic particle diameter). The relaxation times defined in Eqs. (2.21) and (2.22) are typically on the order of 10^{-5} – 10^{-9} seconds [9].

The effective relaxation time is given by the expression [30]:

$$\tau = \frac{\tau_N\tau_B}{\tau_N + \tau_B} \qquad (2.23)$$

In a real FF, any relation between τ_N and τ_B is possible. Figure 2-5 shows a comparison between Brownian and Neel relaxation times for a typical FF [25]. Since τ_N increases exponentially with the increase of the particles volume V while τ_B is simply proportional to V, the equality $\tau_N = \tau_B$ is fulfilled at a certain particle diameter d_c [27]. For $d<d_c$ (as it is shown in Figure 2-5), it holds the condition $\tau_N \ll \tau_B$, i.e. according to Eq. (2.23), $\tau \cong \tau_N$: FF magnetization relaxes owing to internal diffusion of the particle magnetic moments. If, conversely, $d>d_c$ then $\tau_N \gg \tau_B$ so the Neel process is frozen and magnetization relaxation proceeds via Brownian rotary diffusion of the particles in the liquid matrix, $\tau \cong \tau_B$. The

larger the particle size the better it holds the condition of "freezing up" of the particle magnetic moment into the particle body [28].

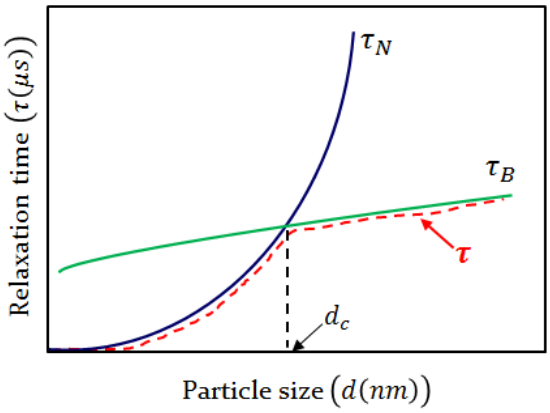

Figure 2-5 The Brownian, Neel, and effective relaxation time constants

When the Neél rotation is the dominant mechanism, i.e., when the magnetic moment is quasi-free to rotate, the particle is super-paramagnetic and so FF (i.e. the magnetization relaxes to the direction of $\vec{H}$ almost immediately (for $d{\sim}(0.3-0.5)\times d_s$ there is $\tau \cong \tau_N{\sim}10^{-9}\ s$) [28].

The opposite case is suspensions of rigid magnetic dipoles (i.e., the grains with "freezing in" magnetic moments, $\tau_N \gg \tau_B$). In this case with the infinitely strong coupling and the finite relaxation time $\tau \cong \tau_B{\sim}10^{-4}-10^{-5}\ s$ the magnetization vector is not obliged to be collinear with $\vec{H}$ which effects of remnant magnetic field in the FF can be seen, and FF besides the magnetic force, can undergo a magnetic torque too.

2.3.3 Curie temperature

The temperature at which all net magnetization is lost is called the Curie temperature, Tc. This temperature is a function of the atomic density, m, material magnetic dipole moment, μ_m, permeability of free space, μ_0, and Boltzmann's constant, k_B [31]:

$$T_c = \frac{m\mu_0\mu_m^2}{3k_B} \tag{2.24}$$

FFs are based on magnetic nanoparticles that are nano scale (so small), they contain only a single magnetic domain. While temperature may not disrupt the magnetic domain in the particles, it can disrupt any alignment between adjacent particles. Thus, FFs experience a similar demagnetization as a function of temperature [29]. Figure 2-6 shows the degradation in magnetization of a magnetic material as a function of temperature.

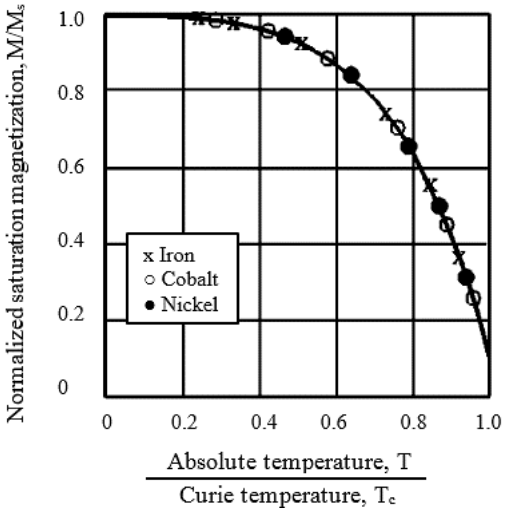

Figure 2-6 Temperature effects on magnetism [8, 29]

2.4 Physical properties of ferrofluids

Generally speaking, the transport properties (viscosity and thermal conductivity) of the FFs are mainly dependent upon the properties, concentration, dimensions and distribution morphology of the suspended nanoparticles as well as the relevant properties of the carrier liquid. Mostly in case of FF with large particles diameter (i.e. $d>d_c$ as described in the previous section), if an external magnetic field is applied, this field exerts a dominant effect on the transport properties, i.e. the field strength and direction will alter the viscosity and the thermal conductivity of the FF.

Thus, the transport properties of this kind of FFs may be strongly anisotropic. However, so far no sophisticated and wide-accepted theory has been found for accurately predicting the viscosity and thermal conductivity values of the FFs [32], and experimental approach is still necessary to determine these parameters [29] for any specific type of FFs.

2.4.1 Viscosity

A FF remains flowable in the presence of magnetic field, even when magnetized to saturation. Nonetheless, the rheology is affected by the applied magnetic field. In the following the viscosity of FFs in the absence and in the presence of an applied magnetic field are discussed.

Due to presence of the suspended particles, the viscosity of the FF is greater than that of the original carrier liquid (in the case of either the absence or the presence of an external magnetic field). This condition is the same as for nonmagnetic colloidal suspensions of solid particles in a liquid [8]. Therefore, theoretical models are available for determining the

viscosity such as Einstein equation [9, 20] which relates the mixture viscosity η to the carrier fluid viscosity η_c and solid particles fraction ϕ (for small concentrations $\phi \leq 5\%$) [8, 19]:

$$\eta = \eta_c \left(1 + \frac{5}{2}\phi\right) \tag{2.25}$$

When a FF is exposed to a magnetic field subjected to shear deformation, the magnetic particles (in regard with their single domain magnetic dipoles) in the fluid tend to remain rigidly aligned with the direction of the orienting field [8]. Accordingly, larger gradients in the velocity field surrounding a particle are to be expected than if the particle is not presented, and so viscous dissipation increases in the sample as a whole. This viscosity increase is more significant in the FFs with large diameter particles ($d_{avg} > d_c$) which Brownian rotational motion develops inside the fluid [8].

Both the strength and direction of the magnetic field play the important roles of affecting the viscosity of the FF [29]. However, when the fluid vorticity and the magnetic field are parallel, the particles can rotate freely and magnetism exerts no influence on the viscosity. While the directions of flow vorticity and magnetic field are perpendicular, the magnetic contribution to the viscosity is maximized [27].

Unfortunately there are no experimental results available for effect of magnetic field on viscosity of the ferrofluid (TMA-250) which is applied in this work, however according to the magnetometer measurements (VSM) and the datasheet (Boron Rubbers Inc.), the resultant behavior of this FF is termed super-paramagnetism (i.e. Neel relaxation mechanism is dominated). As a result, the viscosity of TMA-250 is not significantly affected by the external static magnetic field.

For gaining insight to the dependency of FF viscosity and magnetic field, experimental results for an aqueous magnetic fluid are presented. The ferrofluid which is studied is Fe–water FF (Fe-W FF) that is prepared by the direct mixing method which Fe nanoparticles are mixed with the deionized water by the volume percentages of range from 1.0% to 5.0%. The average particle diameter is 26 nm [29]. In the following, different parameters are discussed and related graphs are presented for the mentioned FF;

I. Effect of the particles volume fraction

As mentioned before, adding nano-particles to a pure carrier liquid increases the fluid's viscosity, whether the magnetic field is applied or not, and it is one of the main factors affecting the viscosity of the FFs. The reason is that an increase of energy dissipation rate occurs during viscous flow due to the presence of the suspended particles [8, 29].

Figure 2-7 indicates the effects of particle volume fraction on the viscosity for the Fe–water FF in the absence and in the presence of a parallel magnetic field. It should be noted that d_c for this type of FFs is about 15 nm [29].

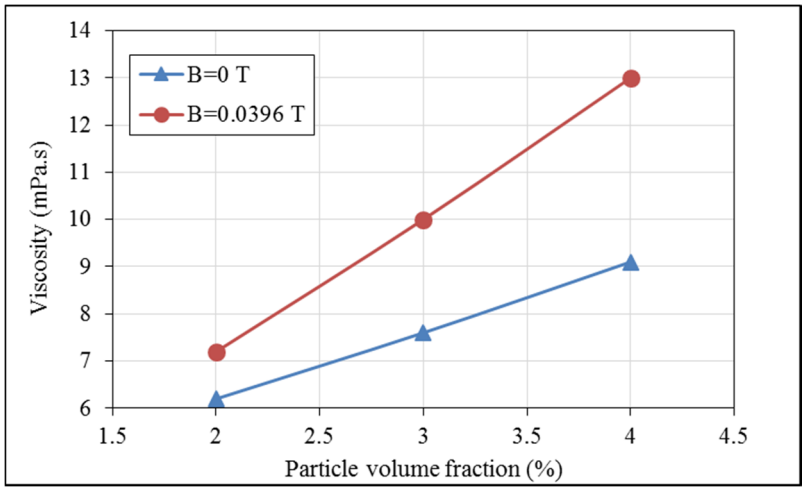

Figure 2-7 Dependence of the viscosity on the particles volume fraction [32]

II. Effects of the surfactant concentration

Besides magnetic nanoparticles and carrier liquid, the surfactants are also involved in preparing a FF. The concentration of the surfactant will affect the distribution morphology of the suspended particles and further affect the viscosity of the FF. This phenomenon is explained by the fact that due to the activator coats on the surface of the magnetic nanoparticles, the interaction between the magnetic nanoparticles and the ambient liquid molecules is intensified. Consequently, the viscosity of the ferrofluid is increased [30]. Figure 2-8 reveals the viscosity of the Fe–water FF of the particles volume fraction 2.0 % with the different activator concentration in absence of the external magnetic field, in which the activator concentration refers to the mass ratio of the activator to the sum of the Fe nanoparticles and the water [30].

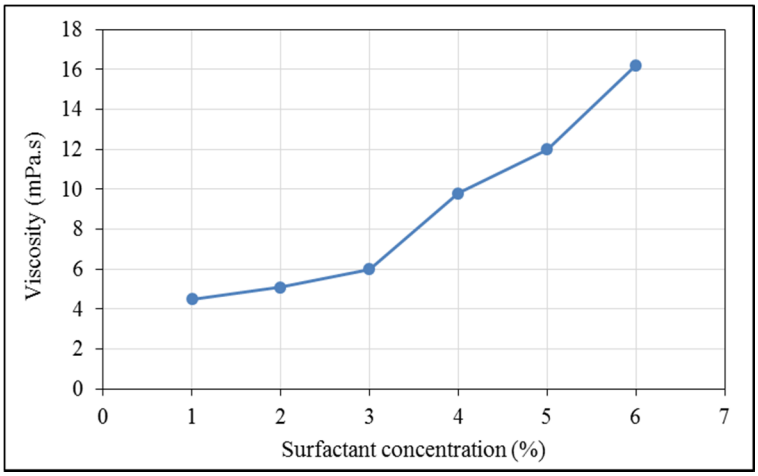

Figure 2-8 Viscosity variation with the different surfactant concentration [30]

III. Effects of the magnetic field strength and direction

Experimental results for this type of FF show the viscosity increases with the strength of magnetic field applied in either the parallel or the perpendicular direction to the flow. Effect of the magnetic field on the viscosity is reinforced with the volume fraction of the magnetic particles. The magnetic particles suspended in the carrier fluid tend to remain chained-alignment along with the direction of the external magnetic field [8, 30]. Here the FF relaxation mechanism should be considered. In case of Brownian relaxation the effects of external magnetic field on the fluid viscosity will be signified as explained before.

Figure 2-9(A and B) illustrates the relative viscosity of Fe–water ferrofluid corresponding to the parallel and perpendicular magnetic fields, respectively. The relative viscosity refers to the ratio of the viscosity of the ferrofluid in the presence of an external magnetic field to that of the ferrofluid in the absence of an external magnetic field.

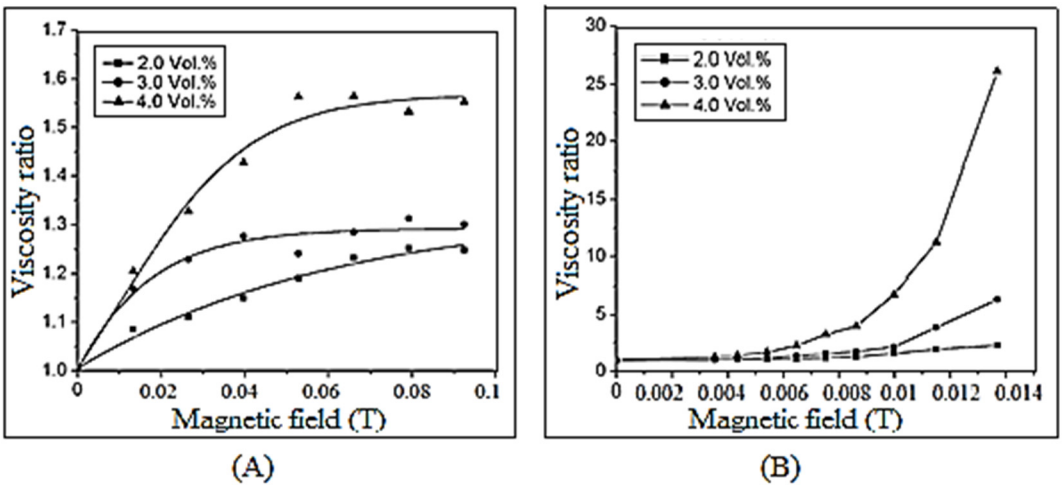

Figure 2-9 Relative viscosity variation with magnetic field, (A) parallel to FF flow (B) perpendicular to FF flow [30]

The reason for difference between Figures 2-9(A), and 2-9(B) is when the FF is exposed to a magnetic field subjected to shear deformation, the magnetic particles in the fluid tend to remain rigidly aligned with the direction of the orienting field [8]. Accordingly, larger gradients in the velocity field surrounding a particle are to be expected than if the particle is not presented, thus viscous dissipation increases in the sample as a whole [8,22].

2.4.2 Thermal conductivity

The suspended magnetic nanoparticles increase thermal conductivity of the suspensions and the FFs have larger thermal conductivity than their base carrier liquids like common nano-fluids. [31].

The magnetic particle volume fraction is one of the factors affecting the thermal conductivity of the FF. For example, 37% increase in thermal conductivity of a kerosene based Mn-Zn ferrite magnetic fluid with 4.5% volume fraction of magnetic nano-particles is reported in

Ref. [20]. Figure 2-10 shows the measured thermal conductivity of the Fe–water FF with the different particle volume fractions in the absence of the magnetic field [31].

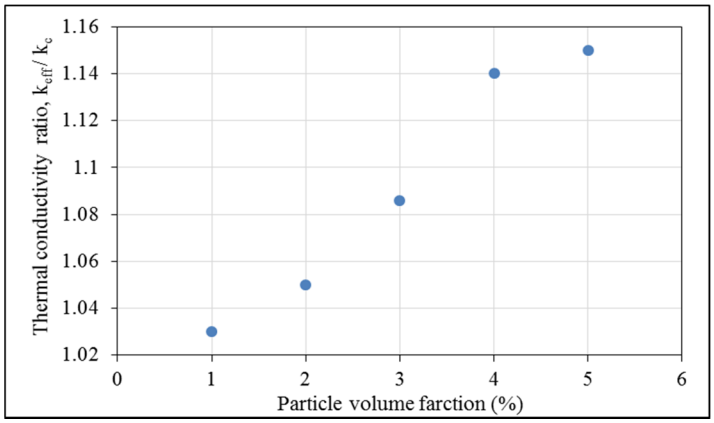

Figure 2-10 Thermal conductivity variation in the absence of magnetic field [31]

In general, the solid particles suspended in the FF form some disperse chain like aggregated structures under the influence of an externally applied magnetic field. Such particles behavior and morphologies determine the characteristics of flow and energy transport inside the FF. Alteration of the magnetic field direction makes the suspended particles into a quite different chain-like aggregation structures corresponding to the orientation of the external magnetic field. Therefore, the orientation of an external magnetic field being relative to the temperature gradient considerably affects the energy transport process of the suspended nanoparticles inside the FF [31]. Figure 2-11(A) illustrates the thermal conductivities of Fe–water FF and pure water in the presence of the external magnetic field perpendicular to the temperature gradient, while Figure 2-11(B) shows the thermal conductivities of both Fe–water FF and pure water corresponding to the magnetic field direction being parallel to the temperature gradient [31].

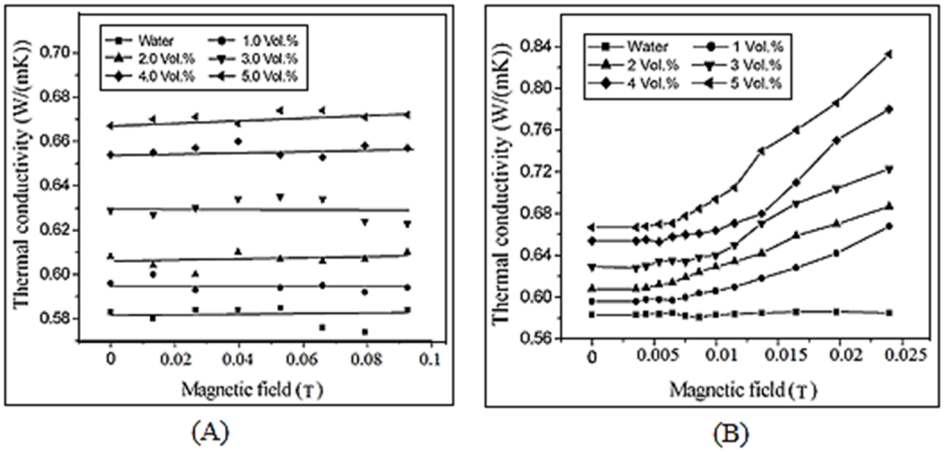

Figure 2-11 Thermal conductivity variation in the magnetic field (A) perpendicular to temperature gradient, (B) parallel to temperature gradient [31]

According to Figure 2-11 and as explained before, when the magnetic field is parallel to the temperature gradient, the particle chains may provide the more effective bridges for energy transport process along the direction of the temperature gradient and enhance heat transfer inside the FF [31]. Also, Figure 2-11 shows thermal conductivity of Fe–water FF increases with the strength of the external magnetic field. In addition, the thermal conductivity raise under the external magnetic field also depends on the concentration of the magnetic particles. The higher the particle concentration, the more remarkable such an increase is.

2.5 Thermomagnetic convection

As already mentioned, ferrohydrodynamics (FHD) explains the fluid dynamic and heat transfer processes associated with the motion of the homogenous, incompressible ferrofluids in the presence of magnetic field and temperature gradients. In general, strong thermomechanical coupling exists when the induced magnetization of the FF is both temperature and field dependent [33].

The most interest in FHD arises from an energy conversion scheme in which heat added to the FF in the presence of a magnetic field is converted into useful flow work with no mechanical pump [9, 32]; magnetically responsive FF composed of nano-scale magnetic particles dispersed in a liquid carrier. The particles which are approximately of domain size remain homogeneously dispersed in the fluid carrier in the presence of magnetic fields or magnetic field gradients (related to their design limitations). When the FF is exposed to the external magnetic field gradient, particles are attracted to the higher intensity region of the magnetic field. While the magnetic force originates within the particles whose number concentration is on the order of 10^{18} per cubic centimeter [9, 32], the particles attempt to slip relative to the fluid and therefore transmit drag to the fluid, causing the dispersion to move as a whole [32].

From electromagnetic theory [34], the force per unit volume on a piece of magnetized material of magnetization $\vec{M}$ in the field of magnetic intensity $\overrightarrow{H}$ is named Kelvin body force (KBF) and is given as:

$$\vec{F}_{KBF} = \mu_0(\vec{M} \cdot \nabla)\vec{H} \tag{2.26}$$

According to paramagnetic characteristic of the FFs (under the influence of magneto-static field) which suspended particles are mechanically free to align with the field in small time compared with the characteristic convection time [32], the direction of magnetization of the fluid element is always in the direction of the local applied magnetic field, thus Eq. (2.26) can be rewritten as:

$$\vec{F}_{KBF} = \mu_0(\vec{M}\cdot\nabla)\vec{H} = \left(\frac{\mu_0 M}{H}\right)(\vec{H}\cdot\nabla)\vec{H} \quad (2.27)$$

where M and H are the scalar magnitudes of magnetization and magnetic field intensity. Using the vector identity and assuming the FF is electrically non-conducting and the displacement current is negligible ($\nabla \times \vec{H} = 0$), Eq. (2.27) is written as:

$$\vec{F}_{KBF} = \mu_0(\vec{M}\cdot\nabla)\vec{H} = \mu_0 M\nabla H \quad (2.28)$$

Eq. (2.28) clearly implies that FHD interactions in FFs require the existence of spatially varying magnetic fields, and also can be influenced by temperature field (because of temperature dependency of the FF magnetization, M=M(T,H)) [9, 32].

Accordingly when the temperature sensitive FF experiences a temperature variation in the presence of an external magnetic field (spatially variant magnetic field), the balance of the induced magnetic body force (KBF) in the FF is broken and a thermomagnetic driving force is produced. This thermomagnetic force causes convective motion of the FF which is called thermomagnetic convection.

2.5.1 Application of thermomagnetic convection in a closed flow loop

Application of the thermomagnetic convection principles in a pipe flow is illustrated in Figure 2-12. As mentioned above, the integration effect of a non-uniform external magnetic field and thermal field on a FF leads to variation in FF magnetic susceptibility and production of the non-uniform magnetic body force (KBF) which results to the thermomagnetic convection [35]; cool FF is attracted to the region with the highest magnetic

field strength. While the temperature of the FF in the heat source section (right end of the magnetic field in Figure. 2-12) increases.

As the FF temperature increases its local magnetization decreases. Then the cooler FF displaces the warmer FF and results in FF flow. This concept can be exploited to circulate the ferrofluid in a flow loop (using only external magnetic field and thermal field gradients) [31]. Such an energy conversion in FFs (in the presence of an external magnetic field) in the closed loop shows promising possibilities for applications in a variety of fields, especially in thermal management of electronic systems.

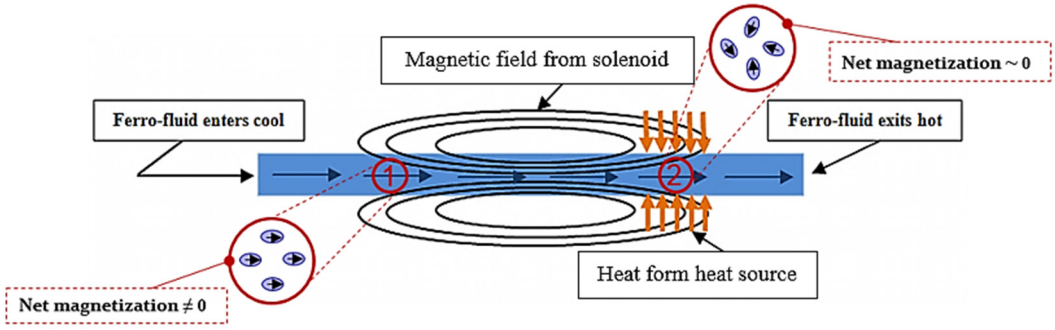

Figure 2-12 Application of thermomagnetic convection in pipe flow

Practical applications of thermomagnetic convection in thermal management of electronic systems require FFs whose magnetic properties are strongly influenced by temperature and as such are referred to temperature sensitive ferrofluids (TSFF) in this work. The TSFFs are chosen such that the material undergoes a substantial drop in magnetization as it approaches the ordinary working temperature of the device to be cooled. As a practical matter, this means that the device's operating temperature is close to or just below the Curie temperature (the temperature at which all net magnetization is lost) of the chosen FF. Use of a FF with a

Curie temperature well above or below the device operating temperature will fail to perform well in the context of the present application [36].

Recently, several efforts have been devoted to the investigation of thermomagnetic convection [11, 20, 24, 37, 38, 40], which demonstrated the feasibility of this kind of energy transport system and revealed its basic features. Results show that the thermomagnetic convection loop (without any moving parts) is a simple design, which is silent, self-driven, self-regulating and maintenance free [11]. In the following a review of some works in this field is presented.

2.6 Literature review

Xuan et al. [11] established the practical design of a liquid cooling device based on the thermomagnetic effect for electronic cooling in which the waste heat generated from the electronic elements was used as a useful power to drive the magnetic fluid flow and to transport the waste heat to a distant radiator. They found that the thermomagnetic cooler with a magnet located nearby the heat source could realize a better cooling performance and a steadier start-up procedure. They also emphasized on the advantages and disadvantages of thermomagnetic cooling for electronic cooling applications. Figure 2-13 shows the prototypes of the coolers investigated in this work.

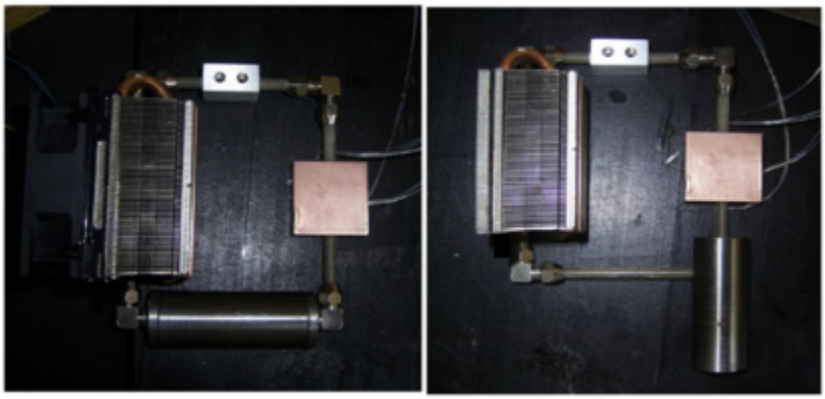

Figure 2-13 Prototypes of thermomagnetic coolers [11]

Lian et al. [20] developed a design method for automatic energy transport devices using a mathematical model for the prediction of flow and heat transport features of the temperature-sensitive magnetic fluid and thermomagnetic effect. Their results revealed that a stable circulation flow could be maintained in a loop-shape channel in the presence of a proper external magnetic field and temperature gradient of the magnetic fluid. In addition, some studies on the factors affecting the device performance, the magnetic field strength and the fluid temperature difference between the heating section and cooling section were conducted. Figure 2-14 shows a schematic of the flow loop used in this work.

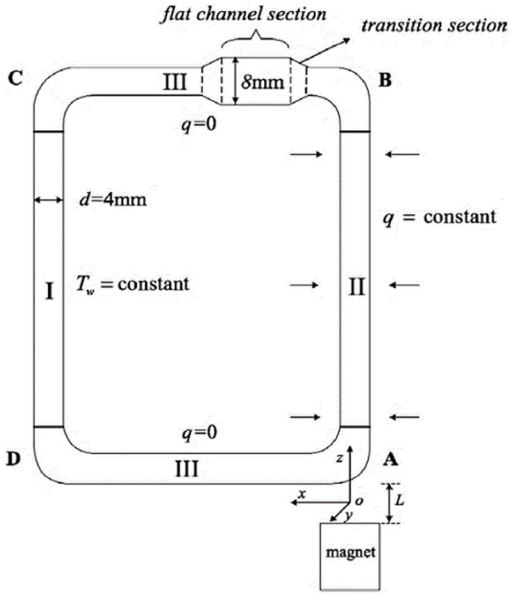

Figure 2-14 Schematic fluid loop used in simulation [20]

Lian et al. [24] experimentally studied the performance of a miniature automatic energy transport device (AETD) based on the thermomagnetic effect of a temperature sensitive magnetic nano-fluid. The investigated device consisted of a permanent magnet, heat source, heat sink and temperature sensitive magnetic fluid assembled into an automatic energy transport device.

A micro-scale particle image velocimetry (PIV) technique was used to visualize the flow field of the magnetic fluid in the loop. By adjusting the external magnetic field and/or temperature gradient field inside the magnetic nano-fluid, they could control the energy transport process of designed device. In addition, the constructed device showed a self-regulating feature that the flow velocity of the magnetic fluid increased with the increase of the heat load and vice versa. Their results also showed that the performance of automatic

energy transport systems was related to the structure of constructed loop. Figure 2-15 illustrates the studied system in this work.

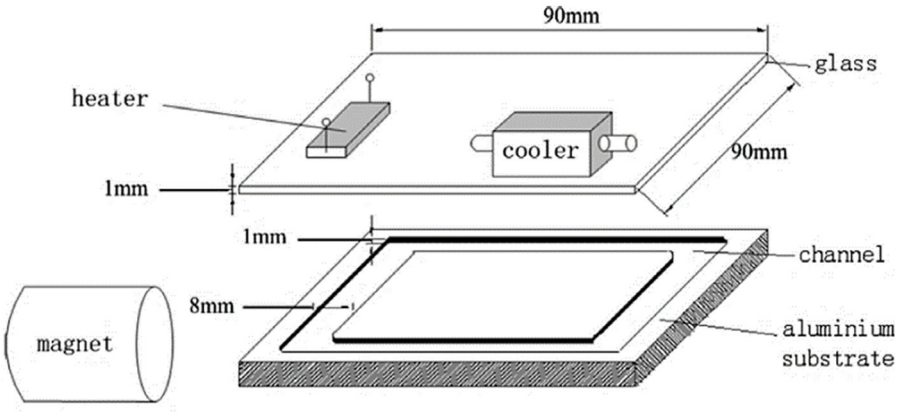

Figure 2-15 Scheme of studied automatic energy transport assembly [24]

Shuchia et al. [37] introduced a binary mixture of a FF and an organic solvent. Effect of magnetic field position on heat transfer and driving force characteristics of this binary magnetic fluid in a heat transport device was investigated experimentally. Their results indicated that the heat transfer capability and the magnetic driving force were improved by magnetic fields when the magnetic field was applied on the entrance of the heated region. Figure 2-16 illustrates the test section which was used in this work.

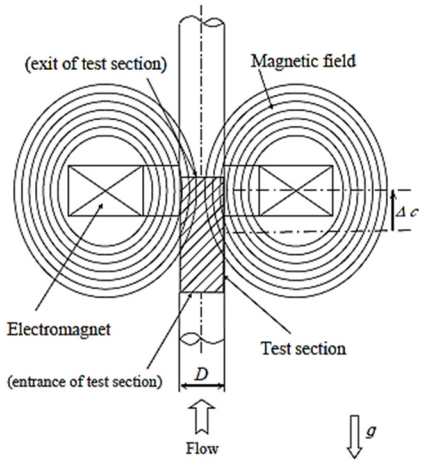

Figure 2-16 A schematic around test section which was used in [37]

Blums et al. [38] studied the heat transfer from a nonmagnetic cylinder to a Mn-Zn ferrite ferrofluid, under the influence of laminar free convection in the presence of uniform and non-uniform magnetic fields directed transversally to the axis of the cylinder. Their results confirmed the additive action of thermo gravitation and thermomagnetic body forces on the heat transfer intensity in ferrofluids. They also showed the heat transfer enhancement attributed to the properties of the FF and the magnetic field gradient. Results of this investigation explained that it was possible to use temperature sensitive FFs to achieve a magnetic Rayleigh number that exceeds the thermo-gravitational Rayleigh number. They also found that a greater magnetic Rayleigh number and a higher heat transfer could be achieved when the magnetic field gradient was increased.

Zablockis et al. [39] investigated thermomagnetic convection in a heated cylinder under the magnetic field of a solenoid experimentally and numerically. They found that the heat transfer under a magnetic field could be increased. However, the solenoid used showed to be

impractical, especially for generating sufficiently strong magnetic fields. Figure 2-17 shows the geometry which was studied in this work.

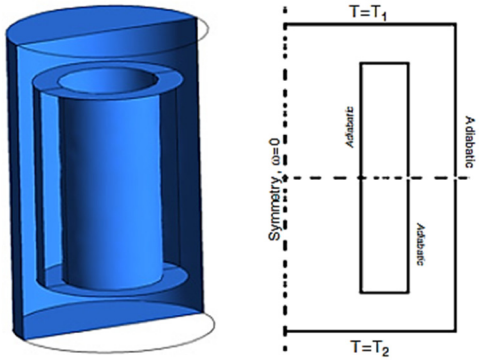

Figure 2-17 Cylindrical enclosure with coaxially positioned solenoid [39]

Yamaguchi et al. [40] conducted an investigation on thermomagnetic convection effect of a Mn–Zn ferrite alkyl-naphthalene based FF in a cubic cavity. The magnetic field and magnetization were affected by temperature, and the greater magnetization and magnetic forces were observed in the regions near the upper wall and center inside the cavity rather than in the region near the bottom and side walls. The analysis of the fluid flow showed a weak flow roll inside cavity under the magnetic force, which brought the lower temperature fluid downward in the center region, and streamed the higher temperature fluid upward along the regions near the side walls. They also found that, with the magnetic field imposed, the heat transfer inside the cavity was increased, compared to that without the magnetic field, and the heat transfer increased further with increasing the strength of the magnetic field.

3 Analytical study

The objective of this chapter is to characterize the thermomagnetic convection in a differentially heated flow loop under the influence of an external magnetic field using dimensional analysis in terms of geometric length scales, magnetic fluid properties, and the strength of the imposed magnetic field. A one-dimensional theoretical model has been developed using scaling arguments to characterize a thermomagnetic circulation loop in terms of physical parameters. A correlation for the non-dimensional heat transfer (Nusselt number) as a function of the appropriate magnetic Rayleigh number and a correlation for the mass flow rate based on the system's properties are developed. Finally, some analysis for magnetic field intensity and heat load limitations are presented.

3.1 Analytical modeling methods

3.1.1 Basic assumptions, geometry and boundary conditions

Analogues to analytical studies of natural circulation systems [41-43], the presented theoretical analysis in this chapter is based on a one-dimensional approach, where the only coordinate runs in the flow direction around the loop, with its origin at the entrance to the heated section. Figure 3-1 illustrates the geometry and the thermal boundary conditions of the rectangular thermomagnetic circulation loop considered in this study. The loop has four sections: i.) a heat source section (q"= constant), ii.) an insulated connecting "hot" section (hot leg), iii.) a heat rejection section (T_{cw} = constant), and iv.) an insulated connecting "cold" section (cold leg).

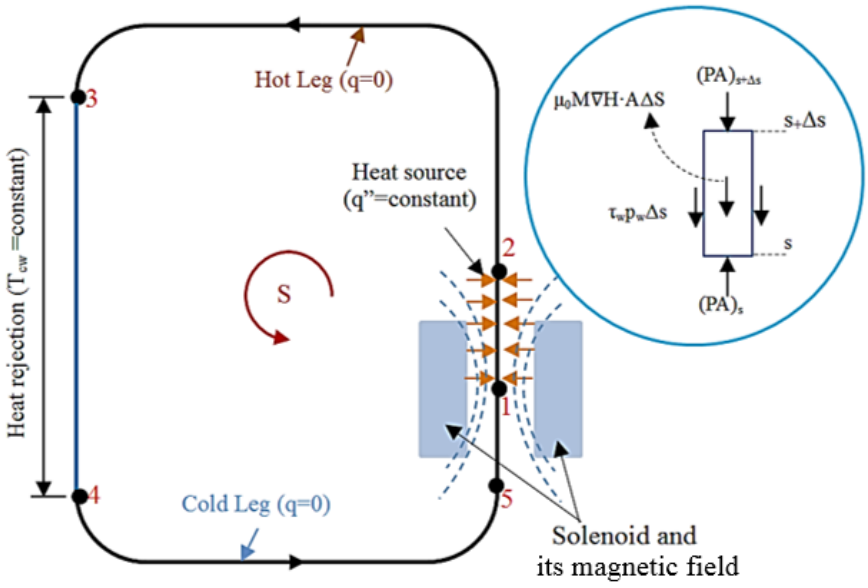

Figure 3-1 Schematic diagram for the rectangular thermomagnetic circulation loop

In this theoretical model the following simplifying assumptions were adopted:

- The average cross section temperature, T, is equal to the bulk temperature.
- Viscous heating and axial conduction effects are negligible in comparison with convection.
- The flow path is composed of constant area flow segments.
- The working fluid is assumed a single phase, incompressible, Newtonian (constant viscosity), electrically non-conductive fluid and its properties are considered constant in the governing equations, except for the fluid magnetization.
- Gravity is neglected (the plane of the loop is normal to $\vec{g}$)

It should be noted that despite the position of the heat source is shown as Figure 3-1 (starting from the middle of the solenoid), no constraint has been exerted in the theoretical model for

this specific heat source position. The only constraint in the theoretical modeling is having the thermal field in just one end of the symmetric magnetic field.

3.1.2 Governing equations

The governing differential equations for 1-D (cross sectional averaged) thermomagnetic driven flow through the loop in the presence of an external magnetic field are as follow:

Equation of continuity:

$$\frac{\partial G}{\partial s} = 0 \tag{3.1}$$

Equation of motion:

$$\frac{1}{\rho A^2}\frac{\partial G^2}{\partial s} = -\frac{\partial P}{\partial s} - \frac{\tau_w p_w}{A} + \mu_0 M \frac{\partial H}{\partial s} \tag{3.2}$$

Equation of energy conservation:

$$GC_P \frac{\partial T}{\partial s} = q"\pi D \qquad \text{Heat source section} \tag{3.3}$$

$$GC_P \frac{dT}{ds} = -h(T - T_{cw})\pi D \qquad \text{Heat rejection section} \tag{3.4}$$

$$GC_P \frac{dT}{ds} = 0 \qquad \text{Connecting tubes} \tag{3.5}$$

where G, s, ρ, A, P, τ_w, p_w, μ_0, M, H, C_p, T, q", D, h and T_{cw} are the mass flow rate (kg/s), axial coordinate around the loop (m), density (kg/m^3), cross section area of tube (m^2), pressure (Pa), wall shear stress at the tube (Pa), perimeter of the tube (m), permeability of vacuum ($4\pi\times10^{-7}$ N/A^2), scalar magnitude of magnetization (A/m), scalar magnitude of

magnetic field intensity (A/m), specific heat of the fluid at constant pressure (J/kg.K), cross sectional averaged fluid temperature (K), heat flux at the tube surface (W/m^2), diameter of the tube (m), convective heat transfer coefficient ($W/m^2.K$), and the wall temperature of the heat rejection section (K), respectively. The last term in Eq. (3.2) is the magnetic force per volume of ferrofluid or Kelvin force (KF), which is the force per unit volume that the ferrofluid experiences in a spatially non-uniform magnetic and thermal field [15].

Independent of magnetic field source, the induced magnetic field inside the ferrofluid which is represented by the vector of magnetic flux density $\vec{B}$ and the vector of magnetic field intensity $\vec{H}$ conform to Maxwell's relations in static form [14]:

$$\nabla\times\vec{H}=0 \tag{3.6}$$

$$\nabla\cdot\vec{B}=0 \tag{3.7}$$

$$\vec{B} = \mu_0\left(\vec{H} + \vec{M}\right) \tag{3.8}$$

Among the properties of the FF, the magnetization, M, is one of the most important properties. For an electrically non-conducting, incompressible fluid this property is a function of the magnetic field intensity and fluid temperature [44, 45]:

$$\vec{M} = K'\vec{H}(T_c - T) \qquad \text{for} \quad T \le T_c \tag{3.9}$$

where K' is the pyromagnetic coefficient (1/K) of the FF and T_c is the Curie temperature (K) (the temperature at which all net magnetization is lost [17]).

Integration of the energy equation for the different segments of the loop yields the cross-sectional averaged fluid temperature distributions as follows:

$$T(s) = \frac{q^{"}\pi D}{C_p G}s + T_{cl} \tag{3.10}$$

$$T(s) = T_{hl} \tag{3.11}$$

$$T(s) = (T_{hl} - T_{cw})exp\left(\left(\frac{h\pi D}{C_p G}\right)(s_{hl} - s)\right) + T_{cw} \tag{3.12}$$

$$T(s) = T_{cl} \tag{3.13}$$

Equations (3.10-3.13) present bulk fluid temperatures as a function of axial position in the heat source section, the hot leg section, the heat rejection section, and the cold leg section, respectively. T_{cl} , T_{hl} and h are bulk fluid temperatures in the cold leg and hot leg (Figure 3-1) sections, and the internal convective heat transfer coefficient ($W/m^2 \cdot K$) in the heat rejection section, respectively.

Integrating the steady state momentum equation, Eq. (3.2) around the flow loop gives:

$$\oint\left(\frac{1}{\rho A^2}\frac{\partial G^2}{\partial s}\right)ds = -\oint\left(\frac{\partial P}{\partial s}\right)ds - \oint\left(\frac{\tau_w p_w}{A}\right)ds + \oint\left(\mu_0 M\frac{\partial H}{\partial s}\right)ds \tag{3.14}$$

Since it is assumed the density and loop cross section are constant, the continuity equation leads to:

$$\oint\left(\frac{1}{\rho A^2}\frac{\partial G^2}{\partial s}\right)ds = 0 \tag{3.14a}$$

Also, by definition the integral of the pressure change around the closed loop is zero:

$$\oint\left(\frac{\partial P}{\partial s}\right)ds = 0 \tag{3.14b}$$

Integration of the second term in the right side of Eq. (3.14) considering both minor (forms) and major frictional losses gives:

$$\oint \left(\frac{\tau_w p_w}{A}\right) ds = \oint \left(\frac{f}{D}\frac{G^2}{2\rho A^2} + \sum_j K_j \frac{G^2}{2\rho A^2} \right) ds \cong \frac{f L_e}{D}\frac{G^2}{2\rho A^2} \tag{3.14c}$$

where:

$$\tau_w = f\frac{G^2}{2\rho A^2} \tag{3.14c-1}$$

$$f = \frac{a}{Re^b} \tag{3.14c-2}$$

$$Re = \frac{GD}{A\mu} \tag{3.14c-3}$$

In Eq. (3.14c) instead of the actual total loop length, L, the equivalent length, L_e, is used for the viscous friction term to account for both minor and major frictional losses [42]. In Eq. (3.14c-2), a and b depend on the flow regime and Re is the Reynolds number, where μ in (3.14c-3) is the dynamic viscosity. The forced flow (i.e. pressure driven) values for a and b, are not generally valid in self-circulation type flows (such as natural circulation or thermomagnetic circulation flow loops) because the driving flow mechanism in these kinds of convection loops is different, the velocity distributions are also different, and these flows are frequently not fully developed [43].

Finally, integrating the last term of momentum equation Eq. (3.14), the magnetic body force over each length of the flow loop and using the FF magnetization as defined in Eq. (3.9), gives the FF magnetic pressure variation as:

$$\Delta P_m = \oint \left(\mu_0 M \frac{\partial H}{\partial s}\right) ds$$

$$= \sum_i \left(\int \left(\mu_0 M(T,H) \frac{\partial H}{\partial s} ds\right)\right)_{L_i} = \left(\int_0^{H_m} \mu_0 M(T,H) dH \right)_{S_5 \to S_2} \quad (3.14d)$$

$$= (\mu_0 \bar{M} H_m)_{S_5 \to S_2} = \mu_0 H_m \left(\bar{M}(T_{cl}) - \bar{M}(T_{hl})\right)$$

$$\bar{M} = \frac{1}{H_m} \int_0^{H_m} M(T,H) dH = \frac{1}{2} K' H_m (T_c - T) \quad (3.14d\text{-}1)$$

$$\Delta P_m = \frac{1}{2} \mu_0 K' H_m^2 (T_{hl} - T_{cl}) \quad (3.14d\text{-}2)$$

The magnetic pressure variation is of interest only in the region between points 5 and 2 (the section of the flow loop which is placed close to the magnetic source) as shown in Figure 3-1. Magnetic effects on the flow in the other sections of the flow loop are negligible in comparison with the magnetic effects in this section.

Note that magnetic body force exerts on the FF to pull that from area outside of the magnetic field to the area with highest level of magnetic field strength. Thus, the integration limitations between 0 and H_m in Eq. (3.14d-1) represent the interaction between magnetic field and magnetisable fluid between the regions outside the magnetic field ($H=0$), and the region with the highest magnetic field intensity ($H=H_m$).

Substituting these integration results into Eq. (3.14), gives that the steady-state motion in a thermomagnetic circulation flow loop as:

$$\frac{f L_e}{D} \frac{G^2}{\rho A^2} = \frac{\mu_0 H^2 K' q}{C_p G} \quad (3.15)$$

which shows that for a thermomagnetic circulation loop in the absence of a gravitational force, friction and thermomagnetic forces play the primary role, without inertia terms. In Eq. (3.15), $q = q^{"}\pi D L_h = G C_p \Delta T_{hs}$ is the total input heat rate (W).

3.1.3 Dimensionless parameters and scaling arguments

Non-dimensional analysis is necessary to compare results from various loops and to extend the theoretical and experimental data from small scale systems to evaluate the performance of large scale loops.

As with natural circulation flow [42, 43], there is no generally accepted approach for selecting characteristic scaling parameters and non-dimensional groups for thermomagnetic convection systems. The primary reason for this is the lack of an unambiguous reference velocity in these flows [42, 43]. For example both the thermal diffusion velocity and the viscous diffusion velocity have been used as the characteristic velocity in non-dimensional thermomagnetic studies [17, 18, 21, 23], however the reasons of choosing these definitions for the characteristic velocity (or the benefits of employing one over the other) are not cleared in the references.

In the following, an effort is made to define the characteristic mass flow rate and the friction coefficient in terms of the flow Reynolds number. Also, the magnetic Grashof number and averaged Nusselt number are correlated using the results from the 1D solution in the steady-state thermomagnetic circulation flow loop (as described in the previous section).

Equation (3.15) gives the mass flow rate in the flow loop as:

$$G = \left(\frac{\mu_0 \, H^2 \, K' q \, D \, \rho \, A^2}{f \, L_e C_p} \right)^{1/3} \tag{3.16}$$

Introducing Eq. (3.16) for the mass flow rate into Eq. (3.10), the temperature difference across the heat source section is found as:

$$\Delta T_{hs} = \frac{q}{C_p\, G} = \left(\frac{q}{C_p HA}\right)^{\frac{2}{3}} \left(\frac{f L_e}{\mu_0 K' D \rho}\right)^{\frac{1}{3}} \tag{3.17}$$

Equations (3.16) and (3.17) give the loop flow rate and temperature difference across the heat source as a function of the primary driving parameters, including the magnetic field strength, the loop geometry, and the fluid properties. These expressions represent first approximations of G and ΔT_{hs}, which can serve as estimates for the steady-state behavior of thermomagnetic circulation loop.

Using Eqs. (3.14c-2 and 3.14c-3), Eq. (3.16) can be rewritten as follows:

$$G = \left(\frac{\mu_0\, H^2\, K' q\, D^{1+b} \rho}{a\, L_e\, C_p\, A^{b-2}\, \mu^b}\right)^{\frac{1}{3-b}} \tag{3.18}$$

Using Eq. (3.18) in Eq. (3.14c-3) gives:

$$Re = A\left(Gr_m \frac{D}{L}\right)^B \tag{3.19}$$

where:

$$A = \left(\frac{1}{a}\right)^{\frac{1}{3-b}}, \quad B = \frac{1}{3-b} \tag{3.20}$$

These equations can be used to obtain an empirical correlation for the friction factor of the thermomagnetic circulation flow.

The non-dimensional group in Eq. (3.19) is the magnetic Grashof number and is expressed as:

$$Gr_m = \frac{\mu_0 H^2 K' q D^3 \rho}{C_p A \mu^3} = \frac{4 \mu_0 H^2 K' q \rho D}{\pi C_p \mu^3} \quad (3.21)$$

As Eq. (3.21) shows, the defined magnetic Grashof number is a function of flow loop geometry (i.e. D), heating load (i.e. q), magnetic field intensity (i.e. H), and the working FF properties (i.e. K′, ρ, C_p, and μ).

Regarding Eq. (3.19), if the steady-state Reynolds number data are plotted versus $Gr_m \frac{D}{L}$ on a log-log graph [42], the related data from different thermomagnetic circulation loops will fall on a straight line with slope equal to *B* and intercept equal to log *A* (i.e. least squares fit), and then parameters *a* and *b* can be evaluated using Eq. (3.20). This method was used by Vijayan et al. [42] to obtain an empirical correlation for the friction factor in a natural circulation flow loop.

Also, heat transfer results can be presented non-dimensionally as average Nusselt numbers for the heat source and heat rejection sections and the modified magnetic Rayleigh number, which are defined, respectively, as:

$$\overline{Nu}_h = \frac{q}{k\pi L_h \left(\bar{T}_{w,h} - \bar{T}_{b,h}\right)} \quad \text{Heat source section} \quad (3.22)$$

$$\overline{Nu}_c = \frac{\bar{h}_c D}{k} = \frac{G C_p}{k\pi L_c} \ln\left(\frac{T_{cw} - T_{b,c,i}}{T_{cw} - T_{b,c,o}}\right) \quad \text{Heat rejection section} \quad (3.23)$$

$$Ra_m = Gr_m \cdot Pr \quad (3.24)$$

Where L_h, $\bar{T}_{w,h}$, and $\bar{T}_{b,h}$ in Eq. (3.22) are the length, the length averaged wall temperature, and the length-averaged bulk temperature of the heat source section, and $\bar{h}_c$, L_c, T_{cw}, $T_{b,c,i}$, $T_{b,c,o}$ in Eq. (3.23) are the average convection coefficient, the length, the wall temperature,

the inlet bulk temperature and the outlet bulk temperature of the heat rejection section, respectively. *Pr* in Eq. (3.24) is Prandtl number.

In the following section, non-dimensional correlations are developed using the numerical simulation results in our 1D theoretical model of the thermomagnetic circulation flow loop. The laminar and steady state 3D numerical models are established using COMSOL Multiphysics version 4.4 simulation software based on the solution of coupled partial differential equations (PDEs) using the finite element method (Chapter 4), and are validated using experimental examinations (Chapter 5) results. The no-slip boundary conditions are applied to the channel walls.

For the thermal boundary conditions, a constant surface temperature is applied to the tube wall in the heat rejection section (heat sink), and a uniform surface heat flux is imposed on the tube wall in the segment where the heat source is placed. The tube walls in other parts of the flow loop are thermally insulated (more details of the numerical and experimental approaches are described in Chapter 4 and Chapter 5, respectively).

3.2 Results and discussion

Once the magnetic field of the solenoid, and the heat source and the heat rejection conditions are prescribed on the loop system, the temperature sensitive ferrofluid commences to flow within the tube driven by the induced thermomagnetic convection driving force inside the fluid. Experimental examinations and numerical simulation results have shown that if all operating conditions are fixed, a stable circulation of the FF can be maintained inside the flow loop at fixed boundary conditions once the whole system starts. The flow and temperature distribution of the FF in the loop is altered by changing the operating conditions of the device.

Looking at the KBF as the thermomagnetic force acting on the temperature sensitive magnetic fluid, it can be found that this force is a function of temperature, and magnetic field gradients. The temperature gradient is a function of the heat source and the fluid and flow properties, while the magnetic field gradient is affected not only by the magnetic properties of the FF medium, but also by the electric current, the number of turns and the spatial distribution of the solenoid. In order to develop friction factor and heat transfer correlations, numerical simulations for 18 different cases were conducted based on different magnetic field strengths, heating rates and the flow loop diameters ($1.8\times10^6 < Gr_m < 3.58\times10^7$) . Table 3-1 presents details of the parameters which were used in the numerical simulations. Also the wall temperature (T_{cw}) of the heat rejection section was maintained at 278 K, and as mentioned before the gravity effect has been neglected.

Table 3-1 Different cases studied numerically

Tube diameter (mm)	Maximum of magnetic field intensity (A/m)	Heat load (W)
4.35	4.4×10^4 (I_s=2 A)	2, 3, 4, 5, 6, 9
4.35	8.9×10^4 (I_s=4 A)	2, 4, 6, 8, 10
6.525	4.4×10^4 (I_s=2 A)	4, 6, 8, 10
8.7	4.4×10^4 (I_s=2 A)	4, 6, 8

Figures 3-2 and 3-3 show the velocity contours and temperature contours at the center-plane of one of the simulated flow (H_m=4.4×10^4 A/m, q=9W).

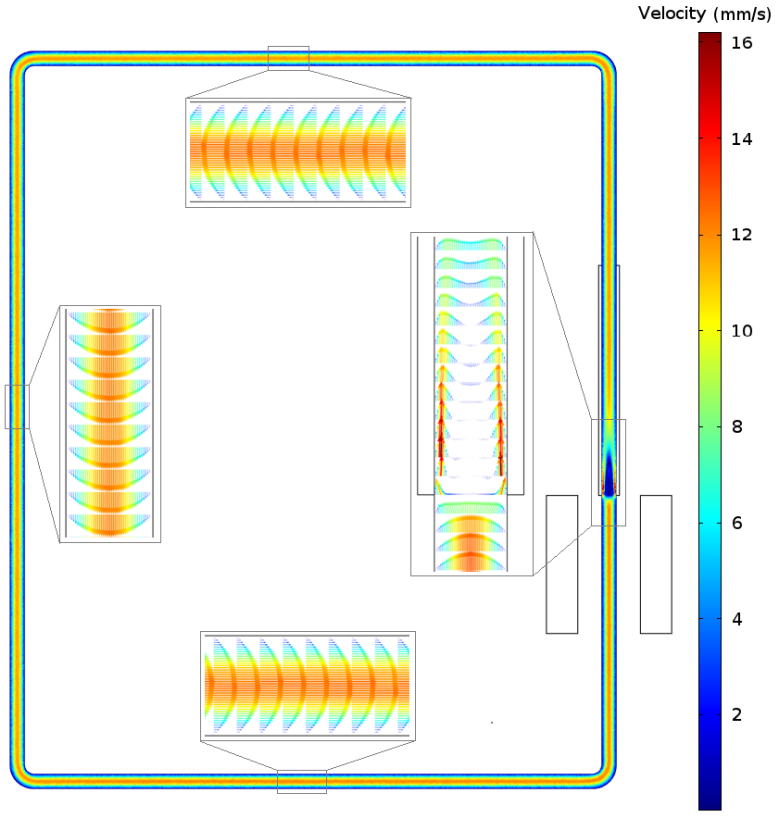

Figure 3-2 Contour and vectors of the center-plane fluid velocity

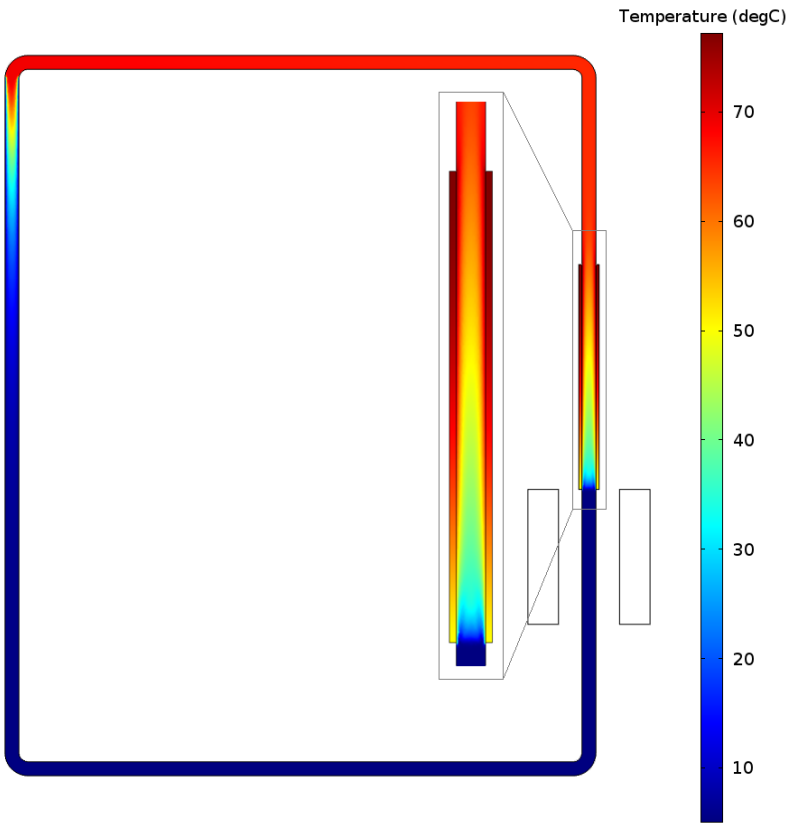

Figure 3-3 Contour of the center-plane fluid temperature

As Figures 3-2 and 3-3 show, temperature sensitive ferrofluid motion occurs due to both temperature and magnetic field gradients, which alter the induced magnetic body force (as explained in Chapter 2 (section 2.5)) and generate the net flow driving force (thermomagnetic convection force) in the flow direction and parallel to the tube axis (in the heat source and the solenoid section of the flow loop, this part can be called the magnetic pump section); the ferrofluid is attracted toward regions with larger field strength, while near the heat source the fluid temperature approaches the Curie temperature of the FF. In this region the fluid loses its attraction to the magnetic field, and is displaced by colder fluid [11, 20, 24].

The numerical simulation results for the 18 steady state flow loop cases are plotted in Figure 3-4 in non-dimensional form. The numerical simulations were validated using the experimental examinations results as explained in Chapter 4.

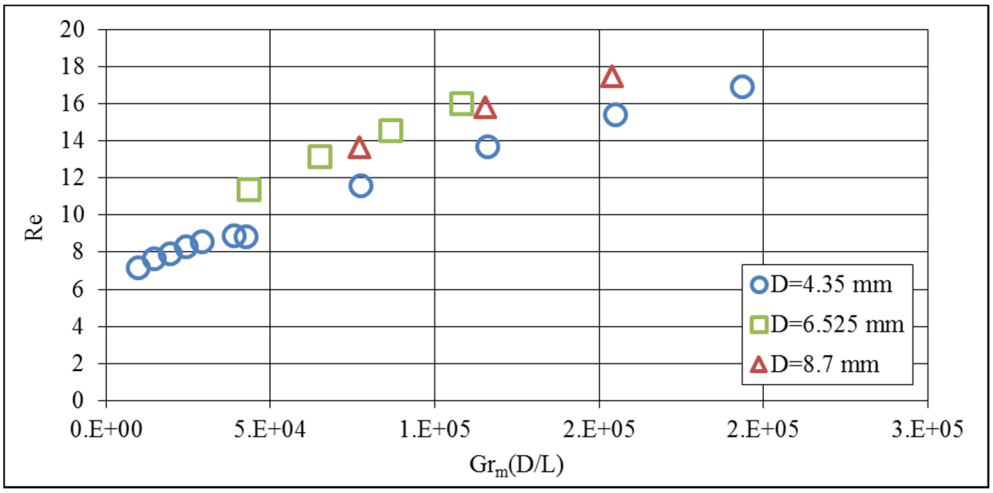

Figure 3-4 Dependence of Reynolds number on product of the magnetic Grashof number and diameter to equivalent length of the flow loop

Using the data shown in Figure 3-4, and Eq. (3.19), a semi-empirical correlation was developed using a least squares fit of the data:

$$Re = 0.3\left(Gr_m \frac{D}{L}\right)^{0.34} \tag{3.25}$$

Employing Eq. (3.20), the following semi-empirical correlation for the friction factor of the thermomagnetic flow in the described loop can be found as:

$$f = \frac{34.5}{Re^{0.06}} \tag{3.26}$$

Figure 3-5 presents the steady-state average Nusselt numbers for the heat source and heat rejection sections for the 18 numerically simulated cases (Table 3-1). In Figure 3-5 blue signs

and red signs denote the Nusselt number for heat source and heat rejection sections, respectively.

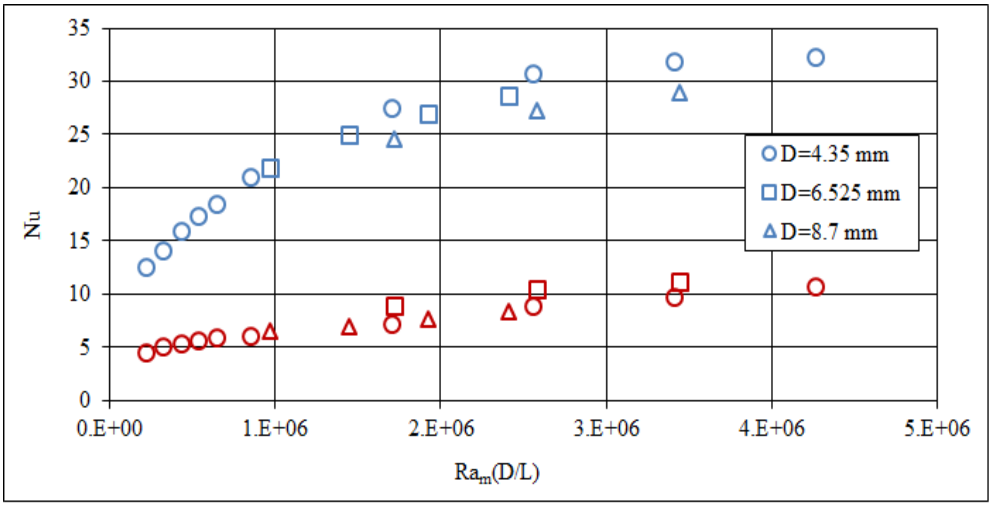

Figure 3-5 Dependence of average Nusselt number on product of the magnetic Rayleigh number and diameter to equivalent length of the flow loop

These results show that the heat transfer in heat source section is much enhanced compared to the heat transfer in heat rejection section (it should be noted that the length of the heat rejection section in these models (and also in the prototype) is about three times longer than the length of the heat source section). This result can be explained by noting the velocity vectors in Figure 3-3; the higher velocity gradient near the heat source walls leads to heat transfer enhancement in this section.

Applying the least squares fit to the data presented in Figure 3-5, semi-empirical correlations for the average Nusselt numbers in terms of product of the magnetic Rayleigh number and diameter to equivalent length of the flow loops for these sections are:

$$\overline{Nu} = 0.25(Ra_m \frac{D}{L})^{0.32} \qquad \text{Heat source section} \qquad (3.27)$$

$$\overline{Nu} = 0.11(Ra_m \frac{D}{L})^{0.3}$$ Heat rejection section (3.28)

3.2.1 Magnetic field intensity and heat load limitations

Since thermomagnetic circulation flow relies on the temperature dependent ferrofluid susceptibility, the magnetic saturation of magnetic fluids presents a limitation for practical applications [13]. Once a ferrofluid is magnetically saturated, strengthening the magnetic field does not further enhance thermomagnetic convection. Therefore, use of these correlations should be restricted to regimes were magnetic saturation does not occur. A derivation of the bounding field strength follows. The magnetization of ferrofluids can be expressed by Langevin equation [15]:

$$M = M_s L(\xi) \quad (3.29)$$

$$L(\xi) = coth(\xi) - \frac{1}{\xi} \quad (3.30)$$

$$\xi = \frac{\mu_0 m H}{k_B T} \quad (3.31)$$

Here, L(ξ) represents the Langevin function. The Langevin parameter ξ is the ratio of magnetic to thermal energies [9]. In this parameter, m and k_B denote the magnetic moment of magnetic particles in the ferrofluid, and Boltzmann's constant, respectively. Assuming that the Langevin equation for ferrofluid magnetization is applicable and that the fluid is nearly saturated for ξ = 100, ((coth (ξ) - 1/ ξ) = 0.99), the value of H that saturates an TMA-250 ferrofluid is about 7×10^6 (A/m). Hence, since $H = \frac{NI}{L_s}$, (N is number of wire turns, I electrical current, and L_s length of the solenoid) a combination of N, I, and L_s values can be used to produce thermomagnetic circulation as long as $\frac{NI}{L_s} \leq 7 \times 10^6 \frac{\mathrm{A}}{\mathrm{m}}$.

Using Eqs. (3.15) and (3.26), an expression for the heat load (W) in the steady state condition can be obtained as:

$$q^{"} = \frac{27.1 L_e C_p \mu^3}{\mu_0 \pi D^3 L_h \rho H^2 k'} Re^{2.94} \tag{3.32}$$

The heat flux load expressed by Eq. (3.32) is considered to be the cooling capacity of the thermomagnetic circulation flow loop. However, considering the critical temperatures for the FF (e.g. boiling temperature of the FF (T_B) or decomposition temperature of the surfactant (T_{sur})), the maximum cooling capacity of the system is determined. It should be noted the Reynolds No. is dependent to the interaction of the magnetic field and the thermal field as described before, and it is not an independent variable.

For TMA-250 as the working FF, the boiling temperature (T_B~150°C) is higher than the decomposition temperature of the surfactant (T_{sur} ~ 100°C), therefore T_{sur} is applied as the critical temperature for defining the maximum cooling capacity of the system:

$$q^{"} < \frac{\mu}{4L_h} C_p (T_{sur} - T_{cw}) Re \tag{3.33}$$

Figure 3-6 shows the cooling characteristics of the thermomagnetic circulation flow loop using Eqs. (3.32) and (3.33) and the results of the numerical simulations. For better understanding of the concept, this Figure illustrates Reynolds No. vs. cooling capacity.

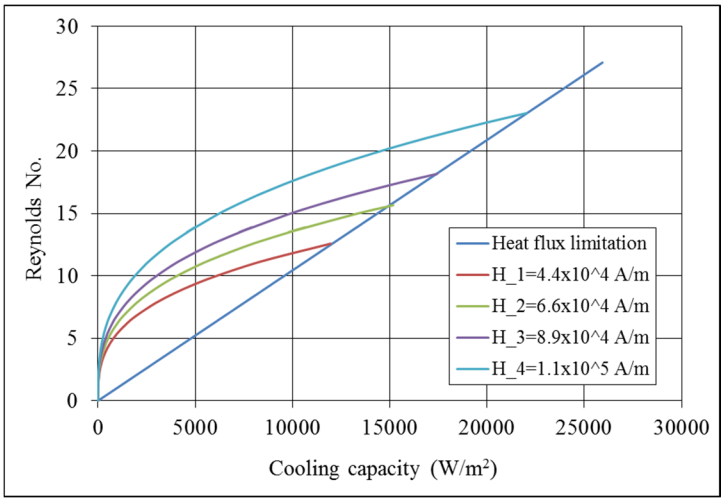

Figure 3-6 Cooling capacity of the thermomagnetic circulation flow loop

Figure 3-6 reveals that the maximum of the cooling capacity of the thermomagnetic circulation flow loop is increased by increasing the magnetic field intensity.

Summary of the analytical approach is presented in Figure 3-7.

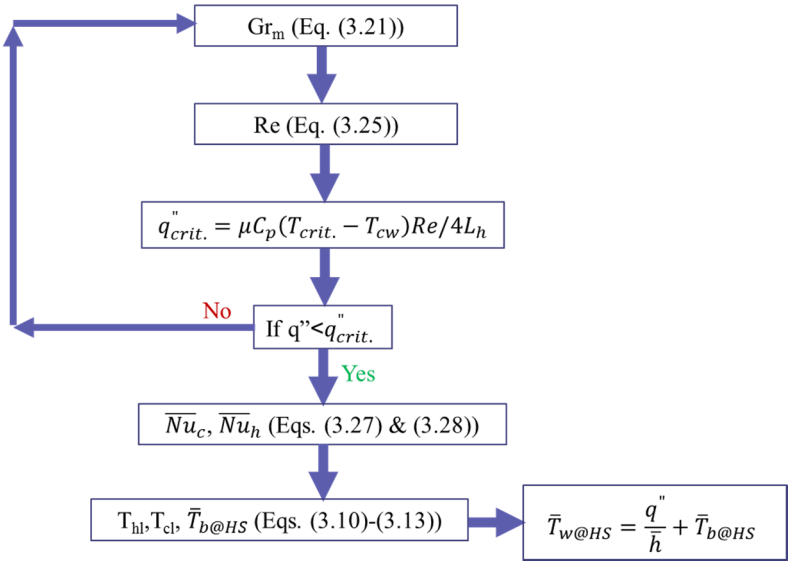

Figure 3-7 Summary of analytical approach

4 Numerical simulation

In this chapter thermomagnetic circulation flow loops are investigated numerically. The three-dimensional, incompressible and laminar simulation models include the heat transfer process from a temperature sensitive ferrofluid contained in a closed flow loop under the influence of an external magnetic field from a solenoid. These models are established using COMSOL Multiphysics simulation software version 4.4 based on the solution of coupled partial differential equations (PDEs) using the finite element method [25], which in addition to standard conservation equations, the magnetic field inside the simulation domain is calculated from Maxwell equations and necessary terms to take into account the magnetic body force have been added to the momentum equation. Therefore presented numerical models of the thermomagnetic circulation flow loops include the coupling of three fundamental phenomena, i.e. electromagnetic, thermal, and fluid dynamic features.

4.1 Mathematical model and numerical simulation

4.1.1 Governing equations

The governing differential equations for simulating the thermomagnetic circulation flow of the single phase temperature sensitive ferrofluid in the presence of an external magnetic field from the solenoid are magneto static field equation, equation of continuity, equation of motion and equation of energy conservation which are explained in the following.

4.1.1.1 Magneto static field equations

Since the magnetic part of this problem is static, Maxwell-Ampere's law for the magnetic field $\vec{H}$ (A/m) and the current density $\vec{J}$ (A/m^2) applies as [46]:

$$\nabla \times \vec{H} = \vec{J} \tag{4.1}$$

Eq. (4.1) is simplified for a non-conducting FF with no displacement current as [15]:

$$\nabla \times \vec{H} = 0 \tag{4.2}$$

Also, the solenoid magnetic field can be determined using the current density in the direction of the wires as [42]:

$$\vec{J} = \frac{NI_{coil}}{A}\vec{e}_{coil} \tag{4.3}$$

where $N, I_{coil}, A,$ and $\vec{e}_{coil}$ are the number of turns, the coil electric current, the total cross section area of the coil domain, and the vector field representing the direction of the wires.

Furthermore, Gauss' law for the magnetic flux density $\vec{B}$ (T) states that [42]:

$$\nabla \cdot \vec{B} = 0 \tag{4.5}$$

Using the constitutive equations the relation between $\vec{H}$ and $\vec{B}$ for FF domain and air domain in the numerical models are defined respectively [15]:

$$\vec{B} = \mu_0(\vec{H} + \vec{M}) \tag{4.6}$$

$$\vec{B} = \mu_0\vec{H} \tag{4.7}$$

Here μ_0 is the magnetic permeability of vacuum ($4\pi\times10^{-7}$ (N/A^2)), and $\vec{M}$ is the FF magnetization.

As explained in chapter 2 (section 2.3) when the FF is exposed to the external magnetic field, the resulting magnetization M is a function of the magnetic field intensity and temperature and it is assumed to be parallel to the magnetizing field H [9, 45]:

$$\vec{M} = M(T,H)\frac{\vec{H}}{H} \tag{4.8}$$

Various relations describing the dependence of M on T and H are proposed in the literature [9, 11, 39, 40]. They are generally in the form of a nonnegative regular function which vanishes for $T \geq T_c$ (T_c is the Curie temperature) [40]. In these cases the magnetization law is generally in this form [9, 39, 40]:

$$\vec{M} = \vec{H} \cdot f(T) \qquad \text{for} \qquad 0 \leq T \leq T_c \tag{4.9}$$

These equations for modeling the FF magnetization are coming from the Langevin formula (as explained in Chapter 2, section 2.3.1) which is the most accurate relation for presenting the magnetization of the FFs. The temperature dependence of the FF magnetization for different cases of applied magnetic field intensity using Langevin function (Eq. (3.30)) is shown in Figure 4-1.

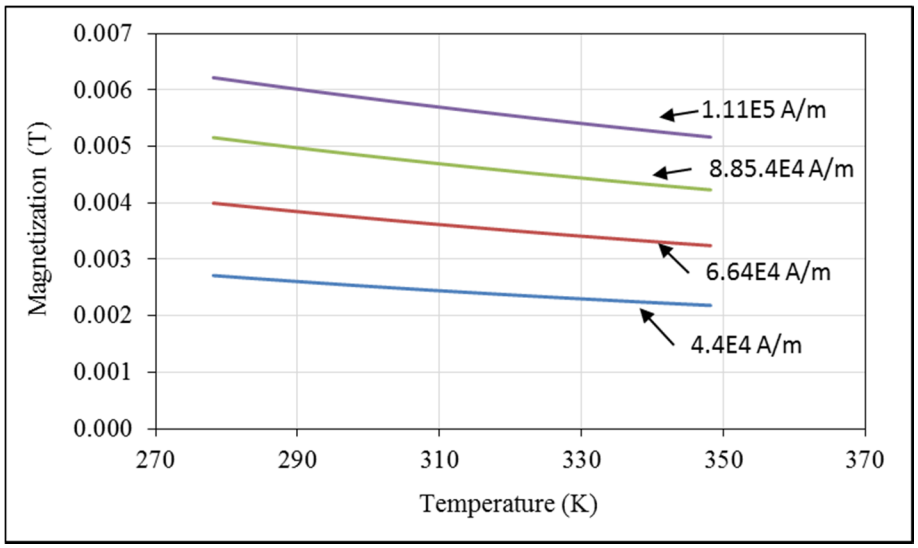

Figure 4-1 Temperature dependence of the ferrofluid (TMA-250) magnetization

As shown in Figure 4-1 magnetization decreases linearly with temperature increasing [44]. These curves can be expressed by a simple equation as [9, 39, 40]:

$$\vec{M} = k'\,(T_c - T)\,\vec{H} \qquad \text{for} \qquad 0 \le T \le T_c \tag{4.10}$$

where k' is the pyromagnetic coefficient which is 0.0028 1/K for TMA-250.

In this thesis Eq. (4.10) is used for modeling the FF magnetization under the influence of thermal field and magnetic field. This expression has been applied in several experimental and numerical investigations in this field before [9, 39, 40].

4.1.2 Ferrofluid motion and energy equations

The governing differential equations for simulating the thermomagnetic convection of the single phase ferrofluid in the presence of an external magnetic field are the continuity equation, the Navier–Stokes equation with Kelvin's body force term, and energy equation [15];

Equation of continuity:

$$\nabla \cdot \vec{V} = 0 \tag{4.11}$$

Equation of motion:

$$\rho\left(\nabla \cdot \vec{V}\right)\vec{V} = -\nabla p + \eta \nabla^2 \vec{V} + \mu_0 M \nabla H \tag{4.12}$$

Equation of energy:

$$\rho C_p\left(\vec{V} \cdot \nabla\right)T = \nabla \cdot (k \nabla T) \tag{4.13}$$

where $\vec{V}$, ρ, p, η, C, μ_0, k, M and H are the velocity vector (m/s), density (kg/m^3), pressure (Pa), dynamic viscosity (Pa·s), specific heat (J/kg·K), permeability of vacuum ($4\pi \times 10^{-7}$ N/A^2), thermal conductivity (W/m·K), scalar magnitude of the magnetization (A/m), and the scalar magnitude of magnetic field intensity (A/m), respectively. The last term in Eq. (4.12) is the magnetic body force or Kelvin body force (KBF), which is the body force per unit volume that the fluid experiences in a spatially non-uniform magnetic and thermal field [15]. Using the above mathematical model, numerical simulations are carried out to study the performance of the thermomagnetic circulation flow loop.

4.2 Basic assumptions, geometry and boundary conditions

To establish a numerical model for the thermomagnetic circulation flow of temperature sensitive ferrofluids, the fluid is assumed as a single phase, electrically non-conducting, incompressible, and Newtonian fluid [15, 20]. This assumption is proper for the description of dynamic phenomena of the FF from a macroscopic view [20].

The working fluid is the temperature sensitive ferrofluid (TMA-250, Boron Rubbers India Inc.) which is used in the experimental works (Chapter 5). Table 4-1 presents the properties of TMA-250 used in the numerical simulations.

Table 4-1 Properties of the ferrofluid (TMA-250)

Density, ρ	Specific heat, C_p	Dynamic viscosity, μ	Thermal conductivity, k	Curie temperature, T_c	Saturation magnetization, M_s
1044(kg/m^3)	1616(J/kg.K)	0.003(Pa.s)	0.16(W/m.K)	348(K)	1.2×10^4(A/m)

Figure 4-2 illustrates the geometry and thermal and magnetic boundary conditions of the rectangular thermomagnetic circulation loop considered in this study. The 4.35 mm diameter tube is used as the fluid channel to form a 21.5 cm × 17.5 cm closed flow loop (like the geometry of the prototype in experimental examinations). As it is shown in Figure 4-2, the loop has four sections: i.) a heat source section (q''= constant), ii.) an insulated "hot" section (hot leg), iii.) a heat rejection section (T_{cw}=constant), and iv.) an insulated "cold" section (cold leg).

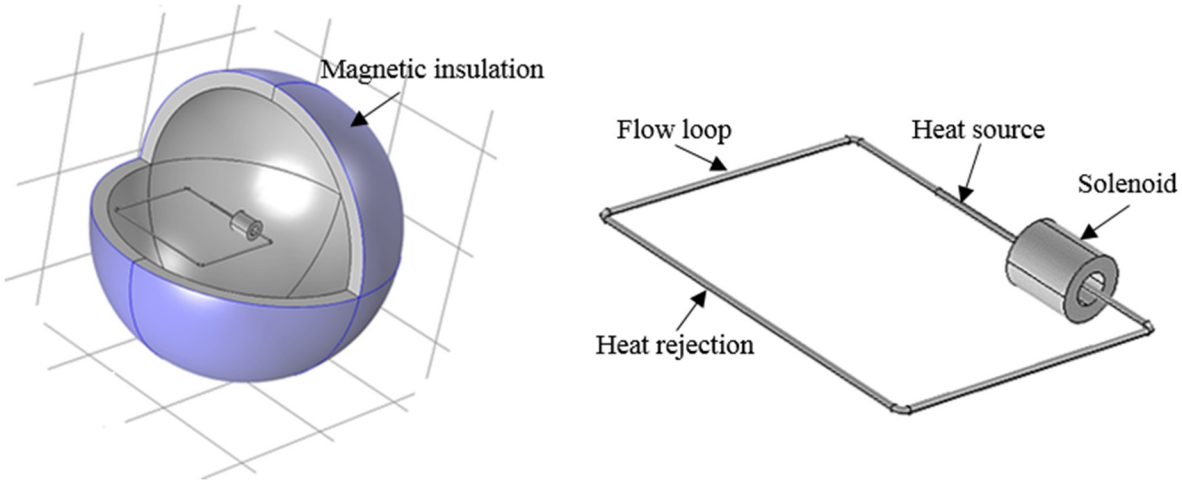

Figure 4-2 Thermomagnetic circulation flow loop, air domain around the solenoid and boundary conditions used in the numerical simulation

As it is shown in Figure 4-2, positions of the heat source section, the heat rejection section, and the solenoid (the solenoid is placed coaxially with the tube), are the same as those used for the theoretical 1-D analysis, and also experimental examinations.

No-slip boundary condition is applied to the channel walls. For the thermal boundary conditions, a constant surface temperature is applied to the tube wall in the heat rejection section (heat sink), and a uniform surface heat flux is imposed on the tube wall in the segment where the heat source is placed. The tube walls in other parts of the flow loop are thermally insulated. The direction of gravity is assumed perpendicular to the flow loop plane, and so its effect has been neglected.

In these numerical models, it is assumed that the solenoid magnetic field is sufficiently strong to be considered constant and all perturbations due to the FF motion can be neglected. Accordingly, the temperature variation in the temperature sensitive ferrofluid will lead to a change in the magnetization and affect the magnetic force acting on the fluid in the presence

of the solenoid magnetic field. The fluid flow affects the convective heat transfer and the temperature distribution inside the magnetic fluid and this in turn affects the driving force on the fluid. Alternatively, the fluid temperature distribution can induce a magnetization variation within the magnetic fluid and thus may vary the driving force.

4.3 Results and discussions

Once the magnetic field of the solenoid, the heat source and heat sink conditions are prescribed on the loop system, the temperature sensitive ferrofluid commences to flow within the tube driven by the magnetic field and the temperature gradient inside the fluid. Numerical simulations have shown that if all operating conditions are fixed, a stable circulation flow of the magnetic fluid can be maintained inside the flow loop at fixed boundary conditions once the whole system starts [20, 47].

The flow and temperature distribution of the magnetic fluid in the loop will be altered by changing the operating conditions of the device [15].

As it was explained in Chapter 2, thermomagnetic convection is a result of the variations of the magnetic body force (KBF) balance acting on the temperature sensitive magnetic fluid. This force is a function of the FF magnetization (which is a function of the fluid temperature and the magnetic field intensity), and the spatially gradient of the magnetic field intensity. Accordingly, using temperature and magnetic field gradients this force and the resulted thermomagnetic convection flow can be modified. The temperature gradient is a function of the heat source, its position in the loop (in regard to magnetic field source) and the fluid and flow properties, while the magnetic field and its gradient are affected not only by the

magnetic properties of the magnetic fluid medium, but also by the electric current, the number of turns and the spatial distribution of the solenoid [15]. In the following contribution of the mentioned factors on the KBF and so the performance of the thermomagnetic circulation flow loop are investigated using numerical simulations.

4.3.1 Validation of the numerical approach

Numerical simulation is commonly used for investigating the physical phenomena in many applications. The quality of the results, however, depends on various factors, like grid quality, boundary conditions and the mathematical model of the phenomenon. For this reason, it is important to validate the performed computation with experimental results. In this part, a comparison of numerical simulation with the experimental examination is performed for the thermomagnetic circulation flow loop (details of the experimental studies are discussed in the Chapter 5).

In order to validate the numerical simulation models, the experimental prototype of the thermomagnetic circulation flow loop has been numerically modeled using the above mathematical model and boundary conditions in COMSOL Multiphysics simulation software. Figures 4-2 and 4-3 schematically depict the geometry of the fluid loop, positions of the heat source section, heat rejection section, and the solenoid involved in the simulations and experiments. The geometry is a 21.5 cm×17.5 cm loop and the diameter of fluid tube is 4.35 mm. Both numerical simulations and experimental examinations of the single phase thermomagnetic circulation flow loop were carried out for a range of heat source powers between 1W and 6W (1100-6728 W/m^2), under the influence of the magnetic field from the

solenoid driven by 2 A electric current. Also, the wall temperature (T_{cw}) of the heat rejection section was maintained at 278 K.

Figure 4-2 illustrates the experimental set up with the positions of the thermocouples in the upstream and downstream of the heat source section (more details about the experimental works are presented in Chapter 5).

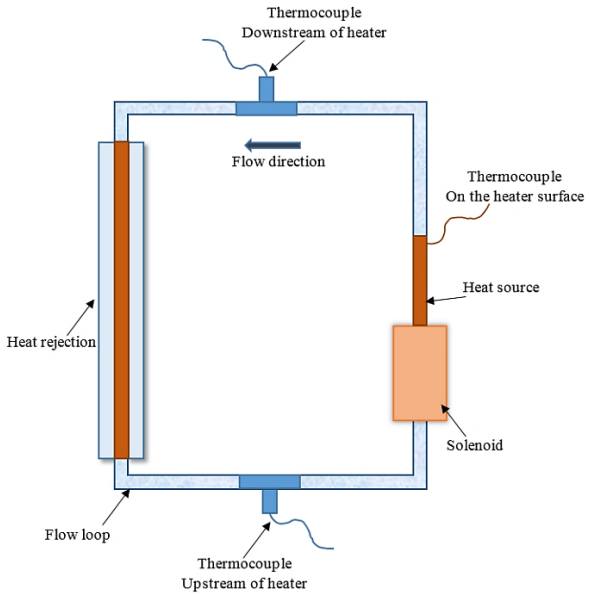

Figure 4-3 Schematic layout of the thermomagnetic circulation flow loop

Figure 4-4 presents the simulated magnetic field for the solenoid in 3D domain and on the center-plane of the flow loop. As this figure shows, the magnetic field intensity is more significant on the part of the flow tube which is placed inside the solenoid and close to that.

Figure 4-5 schematically illustrates the velocity and thermal fields in the flow loop.

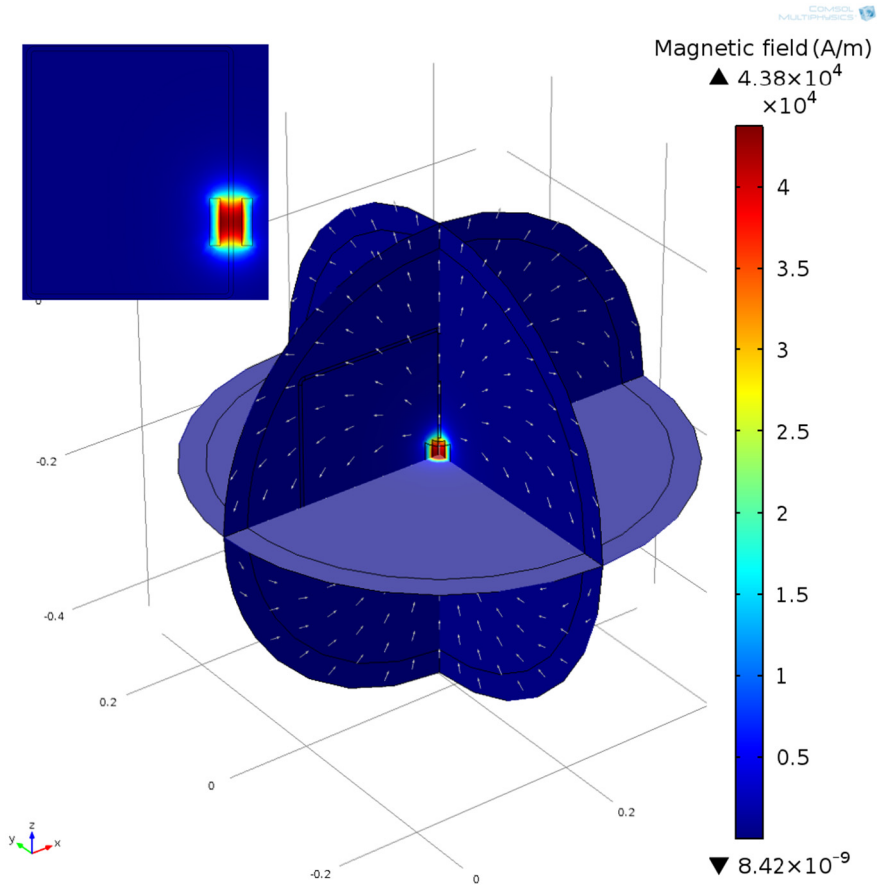

Figure 4-4 Simulated magnetic field of the solenoid (I_s=2 A)

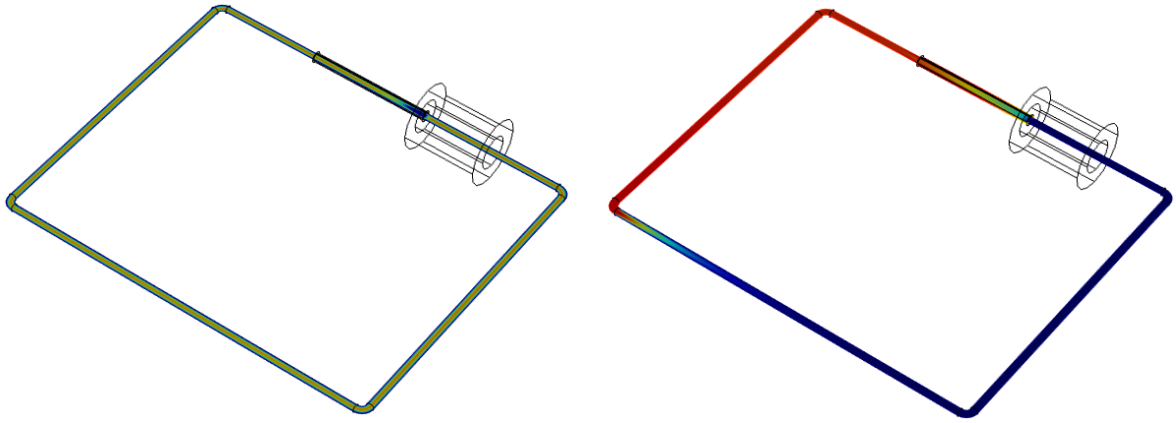

(A) (B)

Figure 4-5 Schematic of the simulated (A) velocity field, and (B) thermal field

Figure 4-6 compares the experimentally measured temperatures and the numerical cross-section average temperatures in the same positions of the thermocouples in the experimental flow loop.

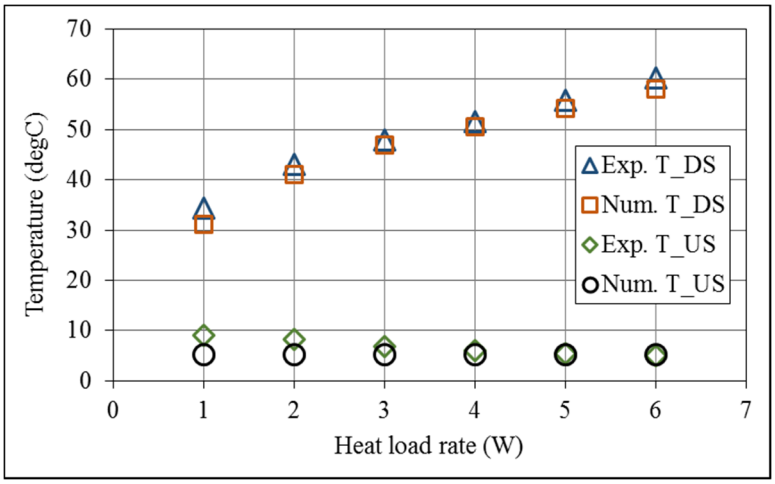

Figure 4-6 Comparison between experimental and numerical temperature results

As Figure 4-6 shows, the numerical and experimental results for the thermomagnetic circulation flow loop are in very good agreement. The average difference between temperature results (downstream (DS) and upstream (US) of the heat source) is less than 5%.

In order to conduct a grid sensitivity analysis for the numerical simulations, three different set of grids with refinement factor of 0.5 (unstructured grid) are selected and the simulation is run for each case. The number of meshes are 262400, 734926, and 1662850. The ratios of the average global cell size, r_{12} and r_{23} (defined as $r = h_{coarse}/h_{fine}$ [48]) are greater than 1.3 which is in the acceptable range of mesh refinement [48]. Using results of these simulations, the Relative Truncation Errors (RTE) are calculated for the flow velocity magnitude as RTE_{1-}

$_2$=0.024 and RTE_{2-3}=0.015 (RTE is less than 5%). Accordingly, the solution appears to be approaching a grid independent value.

Validating the numerical simulation approach with experimental results and also grid sensitivity analysis give us confidence in using the numerical models for studying the effects of different factors on the performance of the thermomagnetic circulation flow loop and also applying associated results in our analytical non-dimensional analysis.

4.3.2 Effect of relative positions of magnetic and thermal fields

In this part, effect of the relative positions of the heat source and the solenoid (magnetic field source) on the performance of the thermomagnetic circulation flow loop have been investigated numerically. As shown in Figure 4-7, six different configurations were studied.

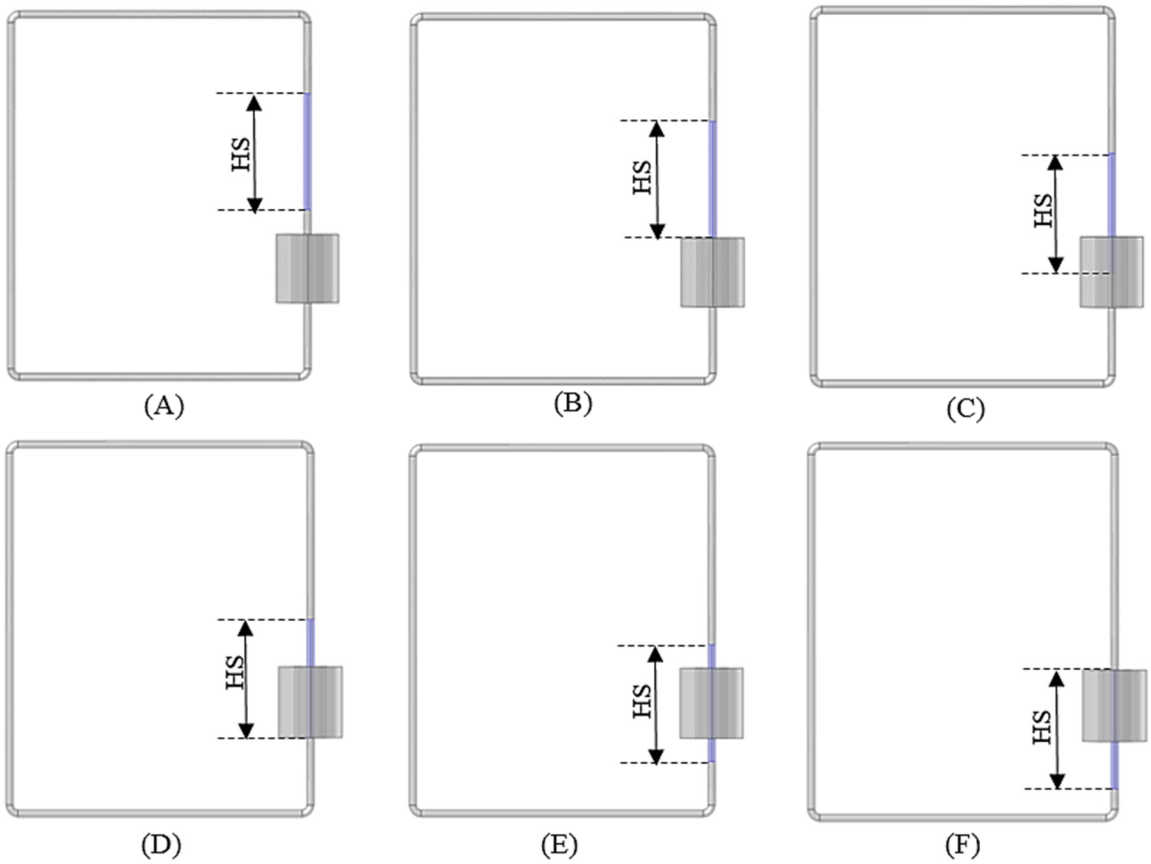

Figure 4-7 Different positions of the heat source (HS) in regard with the solenoid

Associated velocity profiles and average FF temperatures (downstream of HS) of the simulated configurations (Fig. 4-7 (A-F)) were compared in Figures 4-8 and 4-9 (in Fig 4-8, z coordinate denotes tube diameter direction).

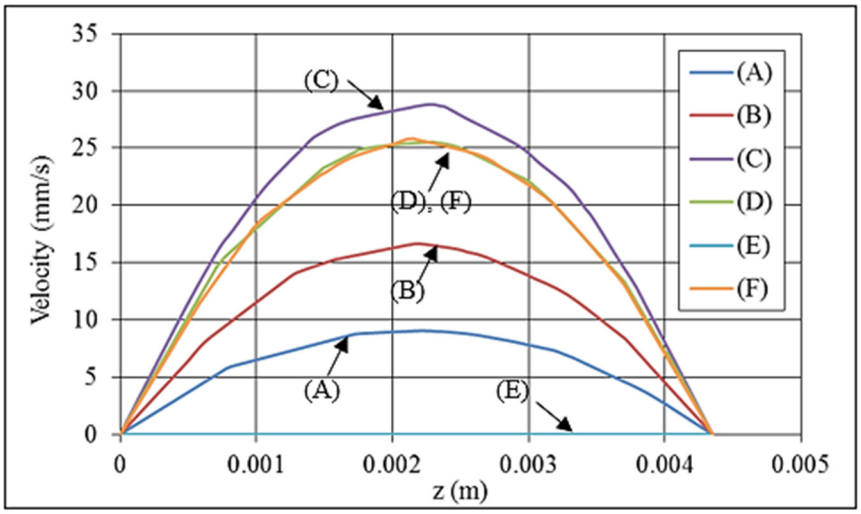

Figure 4-8 Velocity profiles for different positions of the heat source

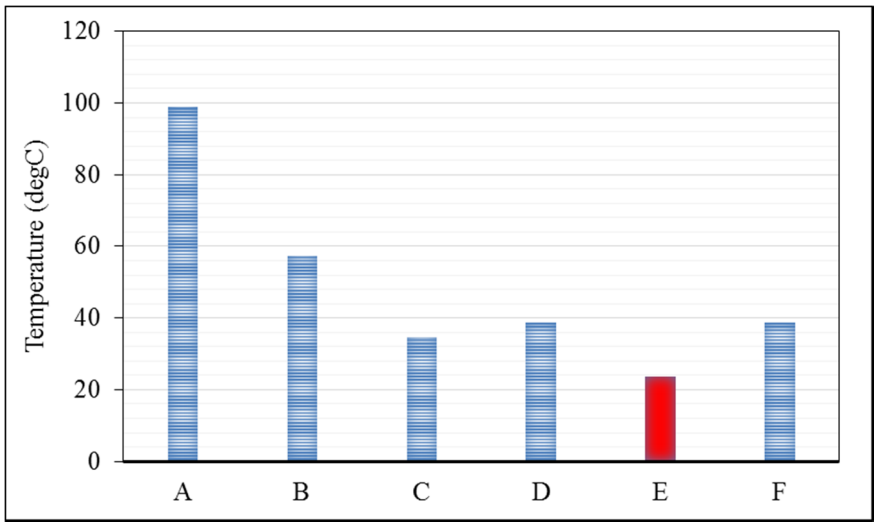

Figure 4-9 Average temperature of the FF (downstream of HS) for different positions of the heat source

Presented results can be explained using the concept of the thermomagnetic convection driving force as explained in details in Chapter 2 (section 2.5). As seen in Figures 4-8 and 4-9, the highest velocity and the lowest average temperature (except case E in Fig. 4-9) are

related to case C (Fig. 4-7(C)), which the heat source is located starting from middle of the solenoid. In this case, there is a good temperature gradient in the FF domain between two ends of the magnetic field which results the strongest thermomagnetic convection driving force. In other word, increasing the thickness of thermal boundary layers, cross-section average temperature of the FF increases in the direction of the fluid flow which makes weaker induced magnetic body force in this end section of the solenoid and thus stronger net thermomagnetic convection driving force is generated.

Figure 4-7(E) presents the configuration at which the solenoid and the heat source are located symmetrically. Thus, the induced magnetic body force in the FF domain is symmetric and results no net force as the thermomagnetic convection force for driving the fluid flow. Figures 4-8 and 4-9 show the resulted velocity and temperature for this case (the associated temperature in Figure 4-9 is related to the initial temperature which was set for numerical simulation, since the fluid was stationary in this case, the initial temperature has not been changed during the solution). Figure 4-10 shows the FF temperature contours on the center-plane of the flow loop for cases C and E.

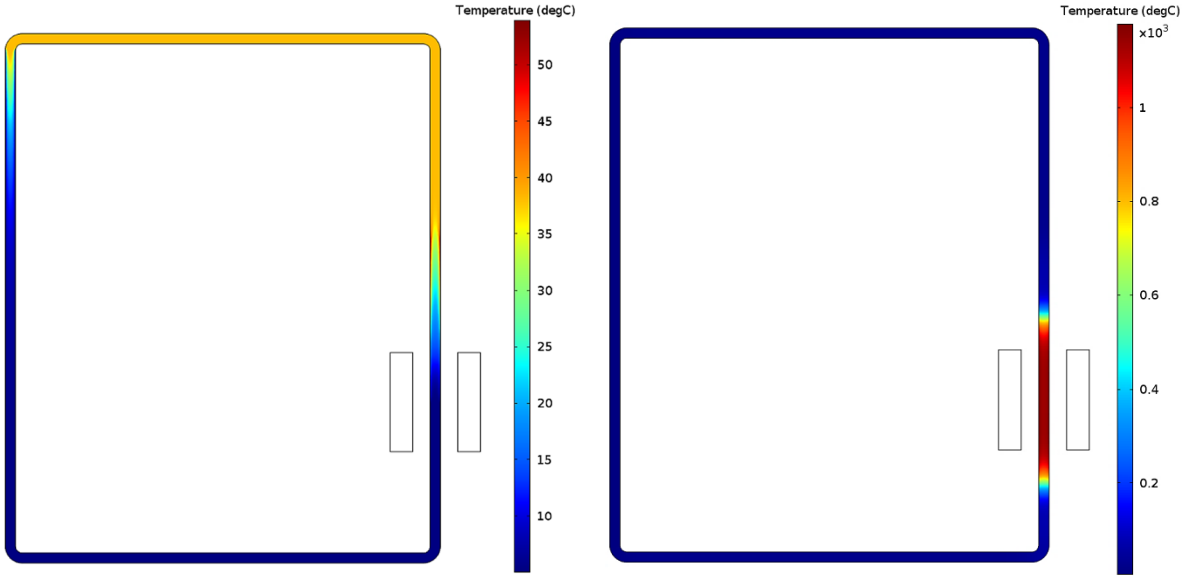

(C) (E)

Figure 4-10 Contours of the center-plane FF temperature for cases shown in Figure 4-7(C and D)

Velocity and temperature results for cases shown in Figure 4-7(D and F) are quantitatively similar (Figures 4-8 and 4-9), however the FF flow circulates in opposite directions in these two cases. In addition, in regard to the relative positions of the heat source and the solenoid in these cases, the temperature gradient between two ends of the magnetic field is less than case (C) which concludes weaker thermomagnetic convection driving force and so lower velocity of the FF flow in the loop.

In the same way, results for relative positions of the heat source and the solenoid as presented in Figure 4-7(A) and (B) can be explained in regard with the temperature gradients between two ends of the magnetic field and the resulted thermomagnetic convection driving force.

5 Experimental examinations

The main goal of this chapter is to present complementary experimental results to our previous analytical and numerical studies carried out on a single-phase, temperature sensitive magnetic fluid (Mn-Zn ferrite based) operating under steady-state laminar flow conditions in a partially heated thermomagnetic circulation loop under the influence of an external magnetic field created by a solenoid. Additionally, this experimental work documents a range of operational conditions for a practical thermomagnetic circulation loop used for electronic cooling. The cooling performance of the device with different magnetic field strengths and heating rates on the heating section are investigated to determine the feasibility of such devices for the thermal management of electronic systems. Furthermore, a self-regulating feature of this cooling system is demonstrated, as the heat load increases a larger heat dissipation rate can be realized due to stronger thermomagnetic convection.

5.1 Thermomagnetic circulation flow loop design and prototyping

An experimental apparatus was used to evaluate the effect of coupling a thermal gradient with a non-uniform static magnetic field (produced using a solenoid) on the performance of thermomagnetic circulation in the flow loop. This experimental setup allows for the measurement of temperature within the FF flow between the heated section and heat rejection section, as well as the temperature of the heat source surface.

The thermomagnetic circulation flow loop is shown schematically in Figure 5-1. Teflon tubes (4.35 mm internal diameter) are used as the primary fluid channel and are combined with

elbows, fittings, a copper heat source tube, and a copper heat rejection section to form a 21.5 cm × 17.5 cm closed flow loop.

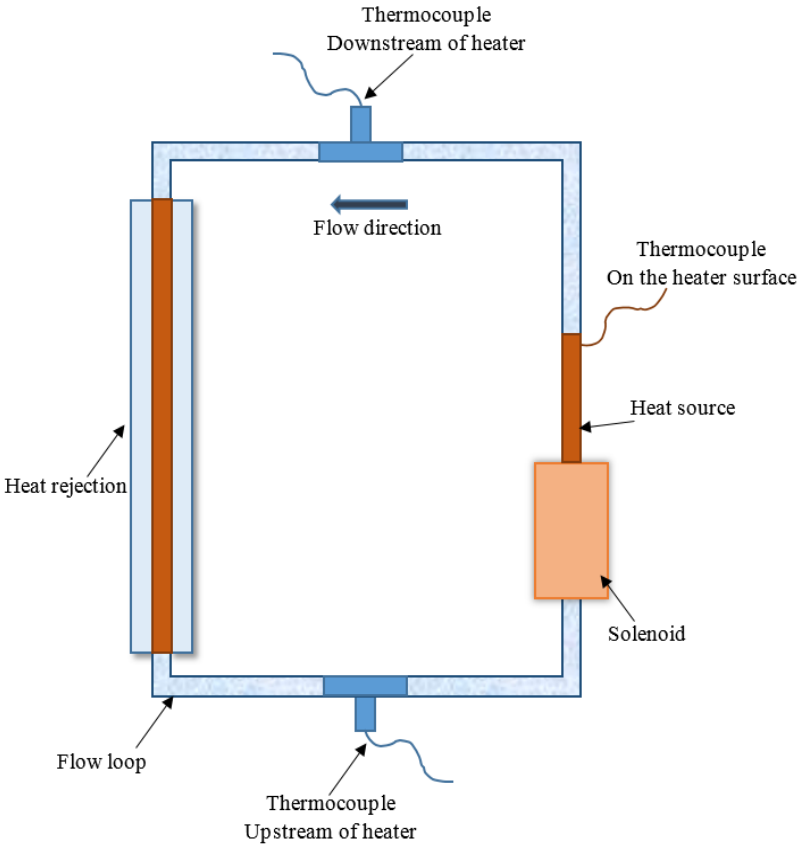

Figure 5-1 Schematic layout of the thermomagnetic circulation flow loop

A solenoid (APW Company) is used as the magnetic field source which is placed close to the heater. Table 5-1 presents the characteristics of this solenoid. A cooling fan and an evaporative cooling setup have been placed for cooling the solenoid which allowed us to apply and investigate effect of higher magnetic fields (i.e. application of electric currents higher than its nominal electric current). Figure 5-2 shows the solenoid and its cooling setup.

Table 5-1 Characteristics of the solenoid

Voltage (V)	6
Current (A)	1.26
Resistance (Ω)	4.75
Wire gauge	23
Turns	800
Bobbin OD (in)	1.5
Bobbin ID (in)	0.75
Bobbin height (in)	1.76

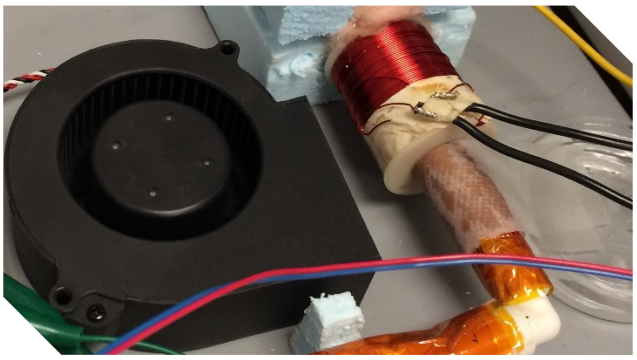

Figure 5-2 Solenoid and its air cooling and evaporative cooling setup

The heat source section is made of a copper tubing (4.35 mm ID), whose OD is electrically insulated using Kapton tape, and is then wrapped uniformly with electrical heating wire (Nichrome wire, NI80.012, R_{wire}=4.182 Ω/ft). Figure 5-3 shows the heat source section.

Figure 5-3 Heat source section

The heat rejection (cooling) section is an annular tube design. It includes a central copper tube (4.35 mm ID) which is part of FF flow loop, surrounded by an outer concentric vinyl tube (ID=15.88 mm, OD=19.05 mm), which allows cooling water to flow in the annulus (as a countercurrent-flow heat exchanger) between the copper and vinyl tubes. The cooling water is provided by a constant temperature water circulator system (Fisher Scientific-Model 801). Figure 5-4 presents a close view of the heat rejection part.

Figure 5-4 Heat rejection section

The flow loop is instrumented with 1 mm diameter, grounded, T-type thermocouples to measure the FF temperature between the heater and heat rejection section as shown in Figure 5-1 (i.e. upstream and downstream of the heat source).

These TCs are positioned to measure the temperatures at the tube center. In addition to these two TCs, a T-type thermocouple (TC) is placed on the copper tube surface of the heat source section (TCs were calibrated using ice-water mixture before using in the experimental studies).

The instrumentation includes three DC voltage sources which provide power to i.) the heat source, ii.) the solenoid cooling fan, and iii.) the solenoid. The TCs are connected to a data acquisition system (Agilent 34970A) for monitoring the temperatures of the system.

A hydrocarbon based Mn-Zn ferrite ferrofluid (TMA-250, Boron Rubbers Ltd., India) is employed as the working fluid. A transmission electron microscopy (TEM) image of the nano-particles in this FF is shown in Figure 5-5 (image was taken in Material Science Department of NCSU).

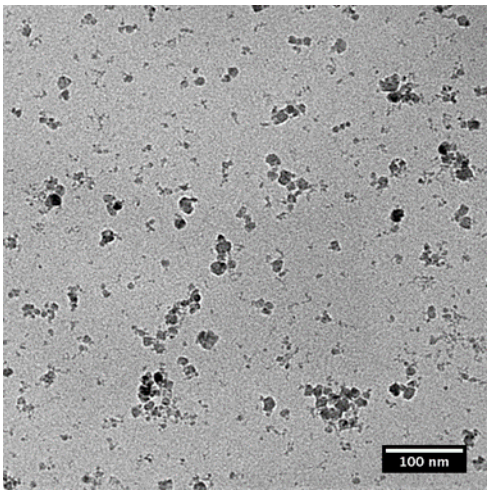

Figure 5-5 TEM image of TMA-250

Table 5-2 presents the characteristics of TMA-250 which are provided by the vendor. Dynamic viscosity of the FF was measured using a viscometer at room temperature as 2.83×10^{-3} Pa.s (Chemical Engineering Department of NCSU) that is in good agreement with the data provided by the vendor.

Besides, specific heat of the FF and its base liquid were measured using a designed calorimetric setup as 1616 J/kg.K and 2073 J/kg.K, respectively.

Table 5-2 Characteristics of TMA-250

<DM>	7 ± 2 nm
σ in ln<D>	0.3
Saturation magnetization, M_s	150 ± 10 Gauss
Fluid density@ 27 ºC	1.044 g/cc
Curie Temp, T_c	75 ±10 ºC
Viscosity η@20 ºC	3.3 ±0.2 cP
Boiling point (of the carrier)	150-300 ºC
Flash point (of the carrier)	37-65 ºC
Magnetic volume fraction	0.0568
Thermal conductivity of TMA250 fluid	157±2 mW/m.K
decomposition temperature of the surfactant	100 ºC
Pyromagnetic coefficient	3.75 G/K
The relaxation mechanism is Neel relaxation base	
The particles are superparamagnetic	

In addition, the magnetization behavioure of the FF in response to the magnetic field at temperature 300 K was measured using vibration sample magnetometer (VSM), results show the superparamagnetic characteristic of this fluid (Figure 5-6).

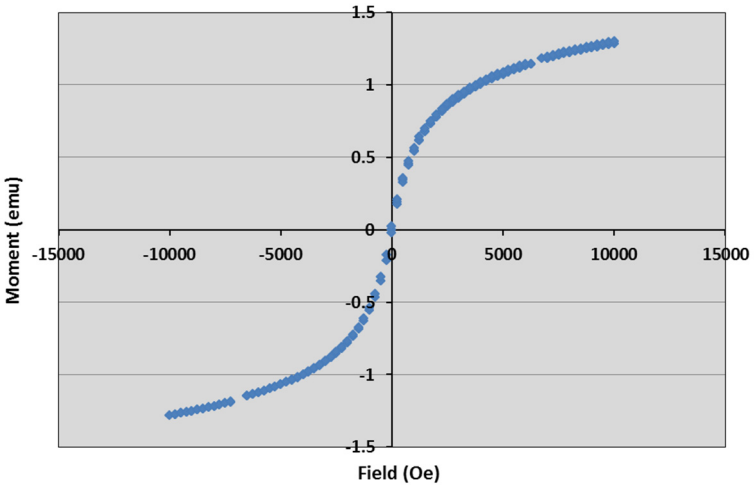

Figure 5-6 VSM data reported at 300 K for the TMA-250

The prototype of the thermomagnetic circulation flow loop is illustrated in Figure 5-7. As shown, a small fan is placed close to the solenoid which is used for its cooling if electrical currents larger than the solenoid's nominal current are used.

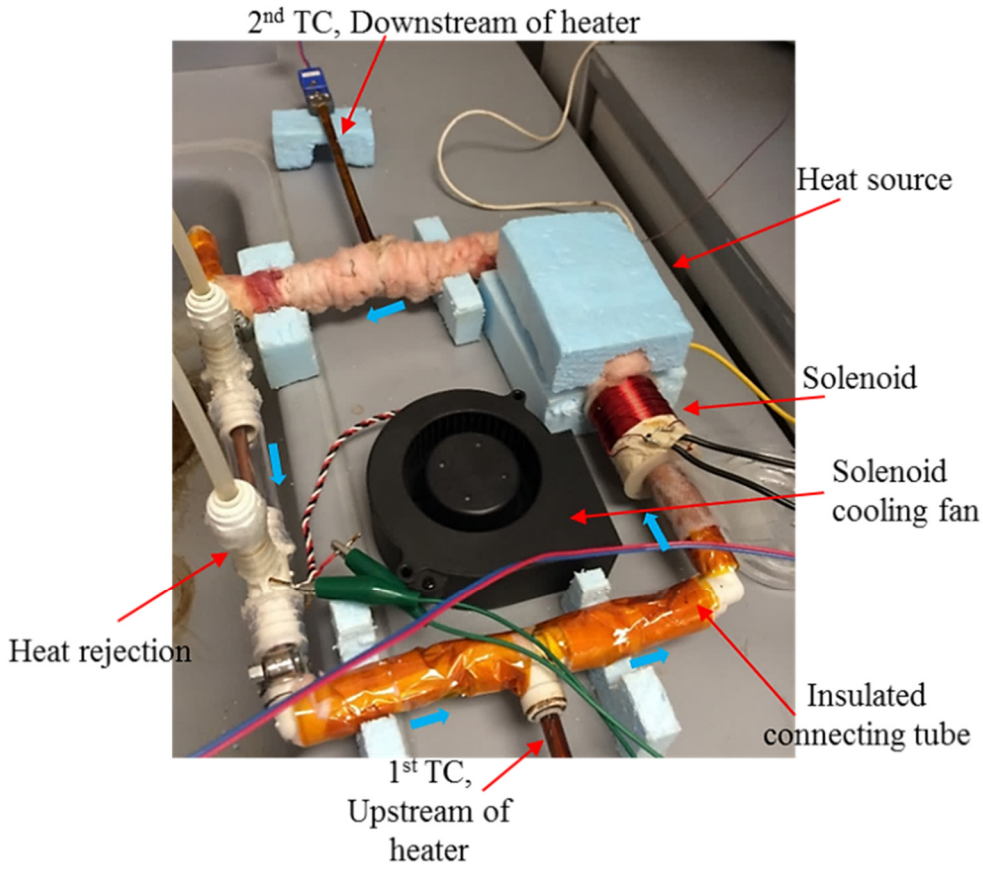

Figure 5-7 Prototype of the thermomagnetic circulation flow loop

Using the presented design, the TSFF inside the loop can easily be driven by the thermomagnetic effect; when the TSFF experiences a temperature variation in the presence of the solenoid magnetic field, the balance of the fluid magnetization is broken and a thermomagnetic driving force is produced.

5.2 Experimental studies

Maintaining the environmental temperature around 25°C and thermally insulating the whole loop using fiberglass insulation (not shown in Figure 5-7), a set of experiments were carried out to investigate the cooling performance of the thermomagnetic circulation flow loop as

described. Throughout all the experiments the prototype was kept horizontal to minimize the impact of buoyancy forces. Also, the temperature of the cooling water in the water circulator tank was kept at approximately 0°C.

Single phase thermomagnetic circulation experiments are carried out in the flow loop for a range of heat source powers between 1W and 6W (1045-6272 W/m^2), at two magnetic field strength using the solenoid.

The first set of experiments were conducted using heat source heating fluxes between 1045 W/m^2 and 6272 W/m^2 and with the solenoid driven by 2 A (theoretical magnetic field strength is around ~3.8×10^4 A/m). Solenoid cooling (fan and evaporative cooling) was used when solenoid currents were greater than 1.26 A (the solenoid nominal current). Figure 5-8 shows the measured temperatures during the start-up of the thermomagnetic circulation in the flow loop. Measured temperatures include i.) the heat source surface temperature, ii.) the FF temperature downstream of the heat source, iii.) the FF temperature upstream of the heat source, and iv.) the temperature of the cooling water inside the cooling water circulator tank.

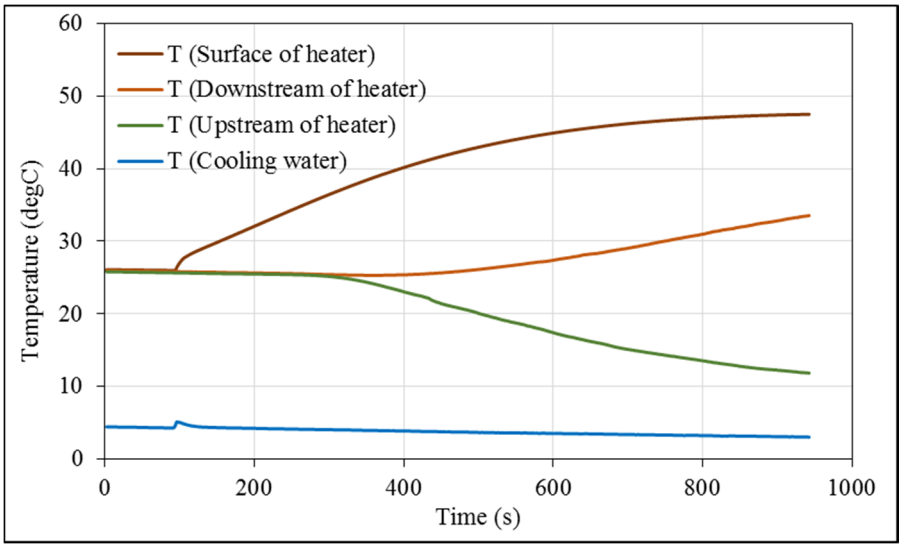

Figure 5-8 Transient temperature history during the start-up of thermomagnetic circulation

Figure 5-8 shows that the heat source temperature rise leads the downstream FF temperature rise during startup. Once temperature gradients form in the FF, thermomagnetic convection starts which leads to the start of heat source cooling. The data in Figure 5-8 show that the rate of source temperature rise decreases once the FF flow starts (around t=300 s). Note that the FF downstream temperature increases as heat is convected from the heat source to the coolant due to FF flow. In addition, the upstream FF temperature decreases due to increased convective heat transfer at the heat rejection section due to FF flow.

The principle of operation was illustrated and explained in Chapter 2 (section 2.5); cool FF is attracted to the region with the highest magnetic field strength. The temperature of the FF in the heat source section increases. As the FF temperature increases its local magnetization decreases (because the FF temperature is approaching the Curie temperature; the temperature at which all magnetization is lost). Then the cooler FF displaces the warmer FF and results in

FF flow and circulation in the flow loop (using only an external magnetic field and internal temperature gradients) [31].

Results of the thermomagnetic circulation flow under heating rates between 1W (1045 W/m^2) and 6 W (6272 W/m^2), and in the presence of the magnetic field from the solenoid with 2A electric current ($H_{max}=3.8\times10^4$ A/m-theoretically) are shown in Figure 5-9. Each heating rate is applied for about 20 minutes.

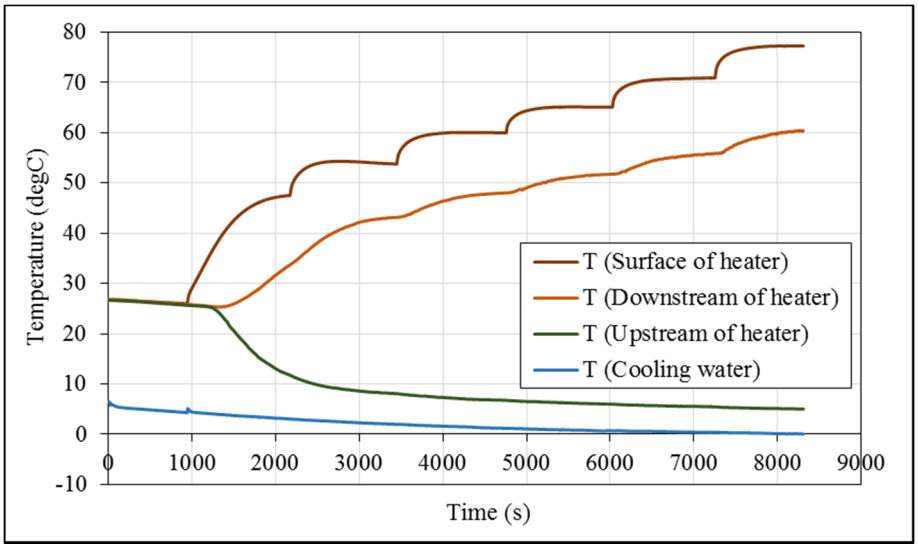

Figure 5-9 Transient temperature history ($I_{solenoid}$=2 A, q=1-6 W)

As seen in Figure 5-9, increasing the heat source heating rate results in an increase in the temperature of the heat source surface and in the temperature of the FF downstream of the heat source. These measurements show that increasing the heating rate by about 6 times, results in a heat source surface temperature increase of 1.6 times in this system. Figure 5-9 also shows that the temperature of the FF upstream of the heat source (exiting from heat rejection section) is decreasing and approaches an asymptotic value.

For the purpose of comparison, another set of experiments were conducted under the same conditions described above except that the electric current of the solenoid was increased to 3A (H_{max}=5.71×10^4 A/m-theoretically).

Results for this experiment are shown in Figure 5-10. These results show that increasing the magnetic field (raising the electric current of the solenoid from 2A to 3A), leads to a decrease in the temperature of the heat source surface by about 10% (for similar heating rates), indicating more effective cooling.

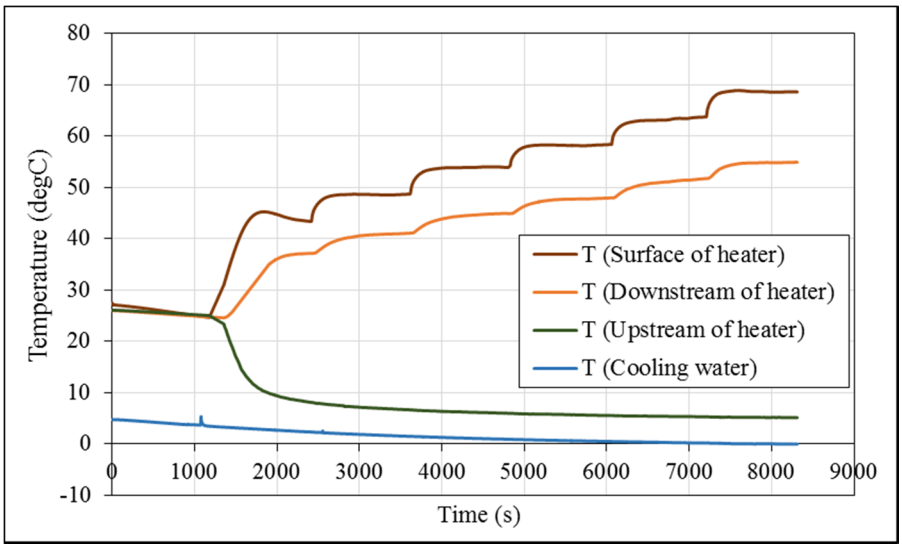

Figure 5-10 Transient temperature history ($I_{solenoid}$=3 A, q=1-6 W)

Additionally, average velocities and Reynolds numbers for each case were calculated using measured temperatures and applied heating rates along with conservation of energy ($Q = \dot{m}C_p\Delta T$). Figure 5-11 shows these results as a function of heat source heat flux (in Figure 5-11, V_2, Re_2 and V_3, Re_3 indicate velocity and Reynolds No. results for the cases where $I_{solenoid}$=2A, and $I_{solenoid}$=3A, respectively).

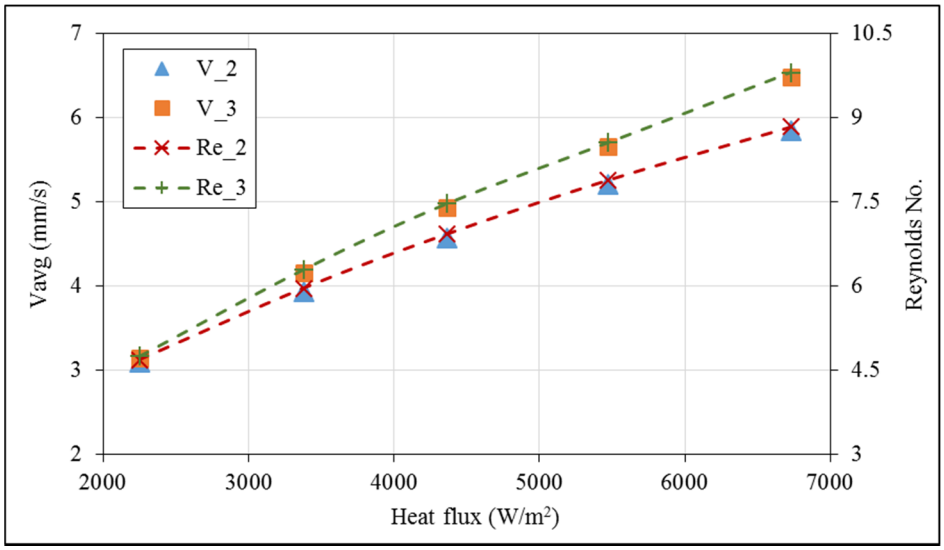

Figure 5-11 Average velocity and Reynolds No. of the TSFF subjected to different heat fluxes for two solenoid electrical currents

Results in Figure 5-11 demonstrate that the flow velocity of the TSFF increases with increasing heat source heat flux (demonstrating a self-regulating feature of thermomagnetic driven flow systems [15, 20]). These results can be explained by noting the larger decrease in the FF's magnetization at higher temperatures (approaching the FF's Curie temperature) which leads to larger net magnetic force gradients [49]. In addition, results in Figure 5-11 show an increase in the FF flow velocity with increasing magnetic field strength (effect of this velocity increase is seen by comparing the heat source temperatures shown in Figures 5-9 (2A solenoid current) and 5-10 (3 A solenoid current) where the heat source surface temperature decreases with increasing electric current of the solenoid for similar heating rates). This behavior can be explained by considering FF saturation magnetization behavior and the Kelvin body force [15]. As the solenoid electrical current is increased, the magnetic field produced by the solenoid increases. Accordingly, the induced magnetic field inside the

FF rises and creates a higher level of magnetization in the magnetic fluid which again results higher magnetic forces giving a larger pressure gradient to drive the flow (more details are given in [49]).

Another interesting result, which can be seen in Figure 5-11, is that the average velocity difference between results of the two magnetic field cases (associated to the solenoid electric currents) increases with increasing heat source heat flux. In order to explain these results, it should be noted that the thermomagnetic driving force is based on the magnetizing and demagnetizing (relaxing) of the FF (using the magnetic and thermal fields). In these processes magnetic energy and thermal energy are competing; either keeping the FF magnetization or demagnetizing it. It appears that at lower levels of input heat flux (i.e. lower temperatures) thermal energy is not high enough to demagnetize the new magnetic alignment of the particles inside the FF under the new higher magnetic field (i.e. 3 A). However increasing the input heat flux, increases the thermal energy (higher temperature) such that the FF magnetization relaxes in the heat source section resulting in higher magnetic force gradients (pressure gradient), and so higher average velocities, and lower heat source temperatures in comparison to the similar conditions with lower magnetic field strength (Figures 5-9 and 5-10) [9].

6 Conclusions

In this study a single-phase, temperature sensitive ferrofluid operating under steady-state laminar flow conditions in a partially heated thermomagnetic circulation flow loop under the influence of an external magnetic field (created by a solenoid) has been investigated analytically, numerically and experimentally as an energy transport device using no mechanical pump with potential applications in thermal management of electronic systems.

In the analytical study a one-dimensional model was developed where the thermomagnetic circulation flow loop has been characterized using scaling arguments in terms of the geometric length scales, magnetic fluid properties, and strength of the imposed magnetic field. Accordingly, a semi-empirical correlation for the non-dimensional heat transfer (Nusselt number) as a function of the appropriate magnetic Rayleigh number and a semi-empirical correlation for the mass flow rate based on the system properties (i.e. Reynolds number versus defined magnetic Grashof number) were developed.

In support of the analytical analysis, the flow and heat transfer in thermomagnetic circulation flow loops were investigated numerically using COMSOL Multiphysics v4.4 simulation software. Numerical results from these simulations were used for developing non-dimensional correlations in the analytical study.

The experimental studies were carried out using a thermomagnetic circulation flow loop filled with a temperature sensitive ferrofluid (TMA-250) operating under steady-state laminar flow conditions under the influence of an external magnetic field.

These experimental measurements documented a range of operational conditions for a practical thermomagnetic circulation loop used for electronic cooling. The cooling performance of the device with different magnetic field strengths and heating rates on the heating section were investigated to determine the feasibility of such devices for the thermal management of electronic systems. The results revealed that the flow in this device can be controlled by the magnetic field and temperature distribution, and that the device possesses a self-regulating function corresponding to the heat source heat rate.

Validation of the numerical simulations using the experimental measurements gave us good confidence to use the numerical simulation models for investigating the thermomagnetic circulation flow loop features. Eighteen different cases (where magnetic field strengths, heating rates and the flow loop diameters were varied) were conducted numerically. Data obtained from these numerical simulations were used as input to create the analytical model to obtain the semi-empirical correlations for non-dimensional flow (Re vs. $Gr_m(D/L)$ where ($1.8\times10^6 < Gr_m < 3.58\times10^7$)) and heat transfer (Nu vs. $Ra_m(D/L)$ where($5.5\times10^7 < Ra_m < 1.1\times10^9$)) which can be used for designing future flow loops. In addition, a methodology for defining the maximum effective range of the magnetic field intensity for a thermomagnetic flow circulation system was presented in terms of the saturation magnetization of the ferrofluid (where for TMA-250 defined as 7×10^6 A/m). Also the maximum cooling capacity of the TMCFL studied here have been defined using system parameters. Results revealed that the maximum cooling capacity of thermomagnetic circulation flow loops are increased by increasing the magnetic field intensity. For the system studied here results showed that using magnetic fields around 10^5 A/m, can transfer a heat flux of 2×10^4 W/m^2 with maximum FF

temperature of ~100 °C. Additionally, the effect of the relative positions of the heat source and the magnetic field source on the performance of the thermomagnetic circulation flow loop have been studied. Results showed that locating the heat source starting from the middle of the magnetic field, produces the highest flow velocity and the lowest average temperature in the thermomagnetic circulation flow loop.

The analytical results showed that the performance of TMCF systems is a function of the ferrofluid properties, magnetic field intensity, and the geometric length scales of the flow loop. However looking at the defined magnetic Grashof number, the most effective parameters are the magnetic field intensity and the viscosity of the FF ($Gr_m \propto \left(\frac{H^2}{\mu^3}\right)$); in this study, a solenoid used to create the static magnetic field. Using a solenoid provided a concentrated magnetic field on the FF flow loop with magnetic field parallel to the flow direction which decreases the field effect on the FF viscosity due to large particles. However, thermal losses (ohmic) in the solenoid limited our ability to apply relatively high magnetic field intensities (higher solenoid electric currents) on our thermomagnetic circulation flow loop. As an alternative magnetic source, permanent magnets have been used in the literature (and also studied in this work). Because of an inappropriate magnetic field configuration, these systems did not show good performance. An extension to this work might be an investigation to determine optimum electromagnetic fields appropriate for this application. In addition, in this work a kerosene based FF has been used with viscosity of 0.003 Pa.s. A water based FF with lower viscosity may improve the performance of this system. Also, optimization studies for defining the most effective distribution of the thermal field coupled

with the prescribed magnetic field configuration is suggested for enhancement of the thermomagnetic effect.

Furthermore our primary studies showed that the velocity of the fluid flow in this system can be improved by using a travelling wave (the same approach which is used for maglev systems), therefore, studying applications of traveling magnetic fields (constant direction) on the performance of the thermomagnetic circulation flow loop would be interesting.

In addition, future works can investigate thermomagnetic cooling of electro-magnetic devices such as the end-windings of electric machines, where the temperature and magnetic field gradients are inherent. Existing thermal and magnetic fields (magnetic leakage field) in this part of the electric machine will provide the energy needed for pumping (circulating) the FF cooling fluid. The cooling mechanism will therefore require no additional moving mechanical parts, pumps, or sensors. The behavior of the fluid will provide the movement (pumping) and cooling of the system (thus increasing energy density and efficiency). Also, since FFs are electrically non-conductive, their electric insulation may be considered for this application. This basic principle can be extended to cooling any media that contains both thermal and magnetic field gradients.

References

[1] Zengerle R., Richter A., Sandmaier H., 1992, "A micro membrane pump with electrostatic actuation", Micro Electro Mechanical Systems Proceedings, An Investigation of Micro Structures, Sensors, Actuators, Machines and Robot, IEEE, pp. 19-24.

[2] Shinozawa Y., Abe T., Kondo T., 1997, "A proportional microvalve using a bi-stable magnetic actuator", Micro Electro Mechanical Systems Proceedings, Tenth Annual International Workshop, IEEE, pp. 233-237.

[3] Stemme E., Stemme G., 1993, "A Valveless Diffuser/Nozzle-Based Fluid Pump", Sensors and Actuators A: Physical, 39(2) pp. 159-167.

[4] Wang B., Chu X., Li E., 2006, "Simulations and Analysis of a Piezoelectric Micropump," Ultrasonics, 44 pp. e643-e646.

[5] Wego A., Glock H., Pagel L., 2001, "Investigations on Thermo-Pneumatic Volume Actuators Based on PCB Technology", Sensors and Actuators A: Physical, 93(2) pp. 95-102.

[6] Benard W. L., Kahn H., Heuer A. H., 1998, "Thin-Film Shape-Memory Alloy Actuated Micropumps", Journal of Microelectromechanical Systems, 7(2) pp. 245-251.

[7] Olsson A., Larsson O., Holm J., 1998, "Valve-Less Diffuser Micropumps Fabricated using Thermoplastic Replication", Sensors and Actuators A: Physical, 64(1) pp. 63-68.

[8] Chalmers D., Fredley J., Kurtz M., 2000, "A new era of instrument thermal management with capillary heat transport systems", 51st International Astronautical Congress, Brazil, pp. 2-6.

[9] Rosenzweig R.E., 1997, "Ferrohydrodynamics", Cambridge University Press, Cambridge, 1985.

[10] Richter A., Sandmaier H., 1990, "An electrohydrodynamic micropump", Micro Electro Mechanical Systems Proceedings, An Investigation of Micro Structures, Sensors, Actuators, Machines and Robots, IEEE, pp. 99-104.

[11] Xuan Y., Lian W., 2011, "Electronic Cooling using an Automatic Energy Transport Device Based on Thermomagnetic Effect", Applied Thermal Engineering, 31(8) pp. 1487-1494.

[12] Jeyadevan B., Chinnasamy C., Shinoda K., 2003, "Mn–Zn Ferrite with Higher Magnetization for Temperature Sensitive Magnetic Fluid", Journal of Applied Physics, 93(10) pp. 8450-8452.

[13] Upadhyay T., Upadhyay R., Mehta R., 1997, "Characterization of a Temperature-Sensitive Magnetic Fluid", Physical Review B, 55pp. 5585-5588.

[14] Banerjee S., Mukhopadhyay,A., Sen S., 2009, "Thermomagnetic Convection in Square and Shallow Enclosures for Electronics Cooling", Numerical Heat Transfer, Part A: Applications, 55(10) pp. 931-951.

[15] Karimi-Moghaddam G., Gould R. D., Bhattacharya S., 2012, "Numerical Investigation of Electronic Liquid Cooling Based on the Thermomagnetic Effect", ASME 2012 International Mechanical Engineering Congress and Exposition, American Society of Mechanical Engineers, pp. 1441-1447.

[16] Raj K., Moskowitz R., 1995, “Ferrofluid-Cooled Electromagnetic Device and Improved Cooling Method”, U.S. Patent No. 5,462,685.

[17] Banerjee S., Mukhopadhyay A., Sen S., 2011, "The Effects of Magnetization Saturation on Thermomagnetic Convection in a Locally Heated Square Enclosure", Numerical Heat Transfer, Part A: Applications, 59(9) pp. 693-718.

[18] Ganguly R., Sen S., Puri I. K., 2004, "Thermomagnetic Convection in a Square Enclosure using a Line Dipole", Physics of Fluids, 16pp. 2228.

[19] Li Q., Lian W., Sun H., 2008, "Investigation on Operational Characteristics of a Miniature Automatic Cooling Device", International Journal of Heat and Mass Transfer, 51(21) pp. 5033-5039.

[20] Lian W., Xuan Y., Li Q., 2009, "Design Method of Automatic Energy Transport Devices Based on the Thermomagnetic Effect of Magnetic Fluids", International Journal of Heat and Mass Transfer, 52(23) pp. 5451-5458.

[21] Mukhopadhyay A., Ganguly R., Sen S., 2005, "A Scaling Analysis to Characterize Thermomagnetic Convection", International Journal of Heat and Mass Transfer, 48(17) pp. 3485-3492.

[22] Niu X., Yamaguchi H., Yoshikawa K., 2009, "Lattice Boltzmann Model for Simulating Temperature-Sensitive Ferrofluids", Physical Review E, 79(4) pp. 046713.

[23] Suslov S. A., 2008, "Thermomagnetic Convection in a Vertical Layer of Ferromagnetic Fluid", Physics of Fluids, 20pp. 084101.

[24] Lian W., Xuan Y., Li, Q., 2009, "Characterization of Miniature Automatic Energy Transport Devices Based on the Thermomagnetic Effect", Energy Conversion and Management, 50(1) pp. 35-42.

[25] Strek T., Jopek H., 2007, "Computer Simulation of Heat Transfer through a Ferrofluid," Physica Status Solidi (B), 244(3) pp. 1027-1037.

[26] Scherer C., Figueiredo Neto A., 2005, "Ferrofluids: Properties and Applications", Brazilian Journal of Physics, 35(3A) pp. 718-727.

[27] Odenbach S., 2002, "Magnetoviscous effects in ferrofluids", Springer Berlin Heidelberg, 2002.

[28] Massart R., 1982, “Magnetic Fluids and Process for Obtaining Them”, U.S. Patent No. 4,329,241.

[29] Franklin T. A., 2003, "Ferrofluid Flow Phenomena", PhD diss., Massachusetts Institute of Technology.

[30] Odenbach S., 2004, "Ferrofluids: Magnetically Controllable Fluids and their Applications", Applied Rheology, 14(4) pp. 179-179.

[31] Love L. J., Jansen J. F., McKnight T. E., 2005, "Ferrofluid Field Induced Flow for Microfluidic Applications", Mechatronics, IEEE/ASME Transactions On, 10(1) pp. 68-76.

[32] Li Q., Xuan Y., Wang J., 2005, "Experimental Investigations on Transport Properties of Magnetic Fluids", Experimental Thermal and Fluid Science, 30(2) pp. 109-116.

[33] Neuringer J. L., Rosensweig R. E., 2004, "Ferrohydrodynamics", Physics of Fluids (1958-1988), 7(12) pp. 1927-1937.

[34] Zahn M., 1987, "Electromagnetic Field Theory: a problem solving approach", RF Krieger Malabar.

[35] Nkurikiyimfura I., Wang Y., Pan Z., 2013, "Heat Transfer Enhancement by Magnetic nanofluids—A Review", Renewable and Sustainable Energy Reviews, 21pp. 548-561.

[36] Leonid B., Segal V., Curran P. C., 2005, "Cooling electromagnetic stirrers." U.S. Patent No. 6,927,510. 9.

[37] Shuchi S., Sakatani K., Yamaguchi H., 2005, "An Application of a Binary Mixture of Magnetic Fluid for Heat Transport Devices", Journal of Magnetism and Magnetic Materials, 289pp. 257-259.

[38] Blums E., Mezulis A., Kronkalns G., 2008, "Magnetoconvective Heat Transfer from a Cylinder Under the Influence of a Nonuniform Magnetic Field", Journal of Physics: Condensed Matter, 20(20) pp. 204128.

[39] Zablockis D., Frishfelds V., Blums E., 2008, "Numerical Investigation of Thermomagnetic Convection in a Heated Cylinder Under the Magnetic Field of a Solenoid", Journal of Physics: Condensed Matter, 20(20) pp. 204134.

[40] Yamaguchi H., Niu X., Zhang X., 2009, "Experimental and Numerical Investigation of Natural Convection of Magnetic Fluids in a Cubic Cavity", Journal of Magnetism and Magnetic Materials, 321(22) pp. 3665-3670.

[41] Ho C., Chiou S., Hu C., 1997, "Heat Transfer Characteristics of a Rectangular Natural Circulation Loop Containing Water Near its Density Extreme", International Journal of Heat and Mass Transfer, 40(15) pp. 3553-3558.

[42] Vijayan P., Austregesilo H., 1994, "Scaling Laws for Single-Phase Natural Circulation Loops", Nuclear Engineering and Design, 152(1) pp. 331-347.

[43] Zvirin Y., 1982, "A Review of Natural Circulation Loops in Pressurized Water Reactors and Other Systems", Nuclear Engineering and Design, 67(2) pp. 203-225.

[44] Matsuki H., Yamasawa K., Murakami K., 1977, "Experimental Considerations on a New Automatic Cooling Device using Temperature-Sensitive Magnetic Fluid", Magnetics, IEEE Transactions On, 13(5) pp. 1143-1145.

[45] Amirat Y., Hamdache K., 2012, "Heat Transfer in Incompressible Magnetic Fluid", Journal of Mathematical Fluid Mechanics, 14(2) pp. 217-247.

[46] Harrington R.E., 2012, "Introduction to electromagnetic engineering", Courier Dover Publications.

[47] Aihara T., Kim J., Okuyama K., 1993, "Controllability of Convective Heat Transfer of Magnetic Fluid in a Circular Tube", Journal of Magnetism and Magnetic Materials, 122(1) pp. 297-300.

[48] Celik I. B., Ghia U., Roache P. J., 2008, "Procedure for Estimation and Reporting of Uncertainty due to Discretization in CFD Applications", Journal of Fluids Engineering-Transactions of the ASME, 130(7) .

[49] Karimi-Moghaddam, G., Gould, R. D., and Bhattacharya, S., 2013, "A Non-Dimensional Analysis to Characterize Thermomagnetic Convection of a Temperature Sensitive Magnetic Fluid in a Flow Loop", ASME 2013 International Mechanical Engineering Congress and Exposition, pp. V08BT09A032-V08BT09A032. American Society of Mechanical Engineers.